Defence Technology 48 (2025) 250–267

Contents lists available at ScienceDirect

Defence Technology

journal homepage: www.keaipublishing.com/en/journals/defence-technology

# Situation maintenance-based cooperative guidance strategy for intercepting a superior target

Xinghui Yan [a], Yuzhong Tang [a], Heng Shi [b,*], Yulei Xu [a], Yiding Liu [c]

[a] Northwestern Polytechnical University, Xi'an 710129, China
[b] Tsinghua University, Beijing 100084, China
[c] University of Hertfordshire, Hatfield AL10 9AB, UK

ARTICLE INFO

*Article history:*
Received 5 November 2024
Received in revised form
18 December 2024
Accepted 23 January 2025
Available online 4 February 2025

*Keywords:*
Cooperative interception
Situation maintenance
Reachability analysis
Virtual target

ABSTRACT

A situation maintenance-based cooperative guidance strategy is proposed to intercept a high-speed and high-maneuverability target via inferior missiles. Reachability and relative motion analyses are conducted to develop and pursue virtual targets, respectively. A two-stage guidance strategy under nonlinear kinematics is developed on the basis of virtual targets. The first stage optimizes the coverage and collision situation by pursuing virtual targets under specific angular constraints. The second stage subsequently intercepts the superior target based on the handover condition optimized by the first stage. Numerical simulation results are provided to compare the effectiveness and superiority of the proposed strategy with those of the reachability-based cooperative strategy (RCS), coverage-based cooperative guidance (CBCG) and augmented proportional navigation (APN) under various maneuvering modes.
© 2025 China Ordnance Society. Publishing services by Elsevier B.V. on behalf of KeAi Communications Co. Ltd. This is an open access article under the CC BY-NC-ND license (http://creativecommons.org/licenses/by-nc-nd/4.0/).

## 1. Introduction

Existing widely studied guidance laws, such as proportional navigation (PN), augmented proportional navigation (APN) and their extensions, are designed to decrease the relative distance under the advantage of the interceptor's maneuverability. However, with the development of aircraft technology in recent years, high-performance missiles and unmanned aerial vehicles have appeared more frequently in the aerial battlefield [1,2]. Without maneuverability advantages, traditional guidance laws confront the problem of unacceptable miss distance (MD) due to acceleration saturation. Therefore, maneuvering targets with the advantages of speed and maneuverability present formidable challenges to the guidance law design. Optimal control, differential game theory, sliding mode control, and coverage strategy are mainly used in the guidance law design for intercepting highly maneuverable targets.

Optimal control is commonly used to determine the control inputs of a system to optimize a certain performance metric and has been widely used to design guidance laws subject to specific constraints. Cottrell [3] designed the first optimal guidance law based on optimal control theory, which considers the first-order dynamics of unmanned aerial vehicles. Weiss et al. [4] designed a guidance strategy by presetting the upper or lower bounds of the miss distance and adopting control effort as a performance metric, which is a more natural and logical objective than minimizing or maximizing the miss distance, thus achieving interception or evasion of maneuvering targets, especially for short flight times. Dun et al. [5] designed a damping term related to the relative distance between the missile and the target in an optimal guidance command, which further optimized the control effort of the guidance process and achieved successful interception of high-speed maneuvering targets. However, although the optimal guidance laws can effectively reduce the miss distance while satisfying the control effort requirements, these guidance laws typically require prior knowledge of the target's maneuvering strategy. The corresponding guidance performance may degrade when quick and accurate acquisition of the target's motion information is unavailable.

Differential game theory, which generates guidance commands at the kinematic level based on the maneuverability of a target, is popular for designing guidance laws for intercepting maneuvering targets. In a missile confrontation scenario, Anderson [6] deduced the optimal analytic expression of a guidance law based on differential game theory, which is less sensitive to errors in the estimation of current target acceleration as compared with the optimal

* Corresponding author.
*E-mail address:* shiheng@tsinghua.edu.cn (H. Shi).
Peer review under the responsibility of China Ordnance Society.

https://doi.org/10.1016/j.dt.2025.01.020
2214-9147/© 2025 China Ordnance Society. Publishing services by Elsevier B.V. on behalf of KeAi Communications Co. Ltd. This is an open access article under the CC BY-NC-ND license (http://creativecommons.org/licenses/by-nc-nd/4.0/).

guidance law. Zhang et al. [7] proposed an adaptive weighted differential game guidance law to intercept a highly maneuvering target. The adaptive weights are adjusted in real time according to the target acceleration estimation error. A zero-sum differential game model was established in Ref. [8], which integrated the relative distance and control effort as the game indicators and formed a guidance strategy under linearized kinematics. Considering the N-to-one interception scenario, Liu et al. [9] proposed a multiple-intelligence differential game method to solve the cooperative guidance problem, which requires less computational effort than the cooperative differential game guidance law and has comparable performance. Refs. [10–13] applied the differential game theory to a three-body confrontation problem in an aircraft active defense scenario. Differential game guidance does not require prior knowledge of the target's maneuvering strategy and is capable of giving full play to the maneuvering capabilities of intercepting missiles. However, these guidance laws mostly rely on linearized kinematics, which can result in performance degradation under high maneuvering and long time-to-go scenarios.

To address the guidance problem under nonlinear kinematics, the active disturbance rejection control (ADRC) method has attracted increasing attention. Hu et al. [14] proposed a terminal time-constrained sliding mode guidance law for intercepting inferior maneuvering targets, which achieves interception via line-of-sight rate shaping. Ma et al. [15] designed a guidance law that is based on the nonlinear ADRC, which regards the uncertainties, such as the target acceleration variation, as total disturbances and compensates for them to improve the interception performance. Based on the performance advantages of intercepting missiles, Refs. [16,17] proposed cooperative guidance strategies based on terminal sliding mode control and augmented proportional navigation, both of which adopted impact time as the coordinating variable. Most ADRC-based guidance laws exploit the speed and maneuverability of interceptors, and the performance is difficult to maintain when facing superior targets.

The coverage strategy can effectively enhance interception performance by covering the target's escape zone with the union of the interception areas of multiple interceptors. In Ref. [18], a reachability-based guidance framework for pursuing evader was proposed based on reachable sets, which geometrically describes the pursuer and evader's moving capability. By uniting the reachable sets of the interceptors and cooperatively covering the maneuvering range of the target, a coverage-based cooperative guidance strategy was proposed in Refs. [19,20] to intercept highly maneuvering targets, which provided the necessary conditions for successful interception under linearized kinematics. In Ref. [21], reachability analysis was employed to obtain a necessary condition for zero-effort miss (ZEM) under nonlinear kinematics, which was further used to optimize the intercept formation against a superior maneuvering target. Liu et al. [22] proposed a coverage-based cooperative guidance (CBCG) law based on three concepts, i.e., interceptor reachable area, interceptor feasible area, and hypersonic vehicle escape area, which can give full play of the scale advantage of low-cost interceptors. Coverage strategy-based guidance methods are suitable for intercepting superior targets and have the potential to handle multiple constraints. However, the existing coverage strategies lack analyses of nonlinear kinematics, the feasibility of interception or coordination indicators.

Before overcoming the problem of intercepting superior targets with coverage strategies, the feasibility of interception should be assessed first. Situation assessment plays a crucial role in estimating engagement results by analyzing the positions, headings, speeds and maneuverabilities of both sides. The resulting engagement window can be regarded as the necessary and sufficient condition for interception and is also referred to as the capture region or attack zone. The existing assessment methods fall into two categories, namely, numerical and analytical methods. Numerical methods usually obtain flight trajectories based on given guidance laws through integration computations and determine the engagement window based on the miss distance. Hui et al. [23] proposed an efficient numerical solving method for establishing a dynamic attack zone for PN laws, which changes with the random wind field after launch. Another dynamic attack zone was established in Ref. [24] based on the Bayesian theory by training the conditional probability table with physical model datasets. However, numerical methods are limited in applications due to the computational burden of finite missile-borne computing resources. In contrast, analytical methods generally have high computational efficiency. Wang et al. [25] compared the capture capabilities of augmented pure proportional navigation (APPN) and retro-augmented proportional navigation (RAPN) guidance against maneuvering targets with a speed advantage. The variations in the capture zone with respect to multiple factors were analytically discussed, including the speed ratio, maneuverability and relative distance. Li et al. [26] derived the maximum acceleration requirements and range of the navigation gain for three-dimensional (3D) realistic true proportional navigation (RTPN). Taking arbitrary maneuvering targets into consideration, a Lyapunov theory-based derivation was conducted, which leads to a 3D capture region based on the closing speed, lateral relative speed and relative distance. However, the above assessment methods focused mainly on weakly maneuvering targets under given pursuit and evasion strategies. When confronted with superior highly maneuvering targets, the corresponding engagement window is either too difficult to obtain or too small for applications given the harshness of the necessary and sufficient conditions for interception. The reachability-based analysis in Ref. [21] offers a novel perspective for situation assessment in terms of the feasibility of the interception problem. Equal-time lines (ETLs) are derived based on the shortest Dubins paths and used as the credible intercept criterion. However, this assessment method focuses solely on analyzing the initial situation statically, and the dynamic process of engagement needs to be studied further.

In addition, Ref. [27] pointed out a flaw in the aforementioned coverage strategies, i.e., even if the target's reachable set is covered by the missile at the initial moment, this coverage situation may be disrupted as the interception process proceeds. If the coverage strategy can be adjusted online based on current information, it can effectively extend the coverage time. Zhang et al. [28] proposed a coverage strategy by taking the target acceleration range as prior information. The interception area of each missile is adjusted online through the target acceleration distribution or the current target acceleration. Guo et al. [29,30] proposed the concept of virtual targets based on reachable sets, which guide missiles to cover real target escape zones dynamically. The introduction of the virtual targets provides a new idea for the online adjustment of the coverage strategy. Motivated by the reachability-based perspective of situation assessment and guidance strategies based on the pursuit of virtual targets, this paper proposes a situation maintenance-based cooperative strategy (SMCS) to intercept a highly maneuvering target via inferior missiles. Reachability analysis is introduced in the arrangement of interceptor formations, which exploits the quantity of interceptors to improve the feasibility of the interception problem. Based on the analysis of relative kinematics, a two-stage guidance strategy is derived to improve the coverage performance of the reachable set and the maintenance of the collision triangles during engagement. The coverage performance is maintained by pursuing virtual targets, whereas impact angle constraints are optimized to improve the formation of the collision triangle near impact. The main contributions of this paper are summarized as follows:

(1) Owing to the nonlinear kinematics adopted in reachability analysis and relative motion analysis, the proposed intercept strategy can be easily extended to various guidance scenarios. In contrast, intercept formation based on the head-on assumption and linearized kinematics [19,20] is difficult to extend to scenarios involving drastic maneuvers and relatively long time-to-go.
(2) Compared with the guidance strategy in Refs. [21,22], the coverage performance during the interception process is improved by pursuing virtual targets, thereby avoiding disruption of the necessary conditions for interception caused by non-maneuvering or weakly maneuvering targets.
(3) Compared with the guidance strategy in Refs. [29,30], the proposed guidance strategy derives an advantageous situation for the formation and maintenance of the collision triangle, which is realized by optimizing impact angle constraints while pursuing virtual targets that effectively improve the guidance performance against a superior highly maneuvering target.

## 2. Problem formulation and analysis

### 2.1. Kinematics equations of motion

For the case of a planar endgame geometry among $n$ missiles and one superior highly maneuvering target, the Cartesian inertial frame is denoted as $X_I - O_I - Y_I$ as shown in Fig. 1. The notations $M$ and $T$ represent the intercepting missile and the maneuvering target, respectively. Both the missiles and the target are assumed to be point masses. The line-of-sight (LOS) range between the $i$ th missile and the target is denoted by $r_i$. $\lambda_i$ denotes the corresponding LOS angle.

The equations of motion and the relevant constraints can be obtained as follows:

$$\begin{cases} \dot{x}_i = V_i \cos\theta_i \\ \dot{\theta}_i = \dfrac{a_i}{V_i} \\ \dot{y}_i = V_i \sin\theta_i \end{cases} \tag{1}$$

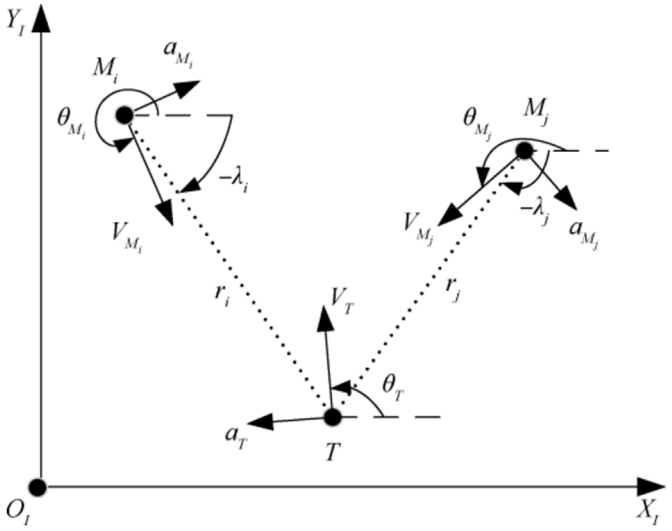


**Fig. 1.** Engagement geometry.

$$\begin{cases} |a_i| \le a_{i,\max} \\ V_T > V_{M_i} \\ a_{T,\max} > a_{M_i,\max} \end{cases} \tag{2}$$

where the subscript $i \in \{T, M_1, \cdots, M_n\}$ represents a specific player, either an intercepting missile or the maneuvering target; $P_i = (x_i, y_i) \in R^2$ is the position of player $i$; $V_i$ and $\theta_i$ are the corresponding speed and heading angle, respectively; $\eta_{M_i}$ and $\eta_T$ are the leading angles, which are equal to the angles between the corresponding heading angle and the LOS. $a_i$ denotes the lateral acceleration and is bounded by the maximum value $a_{i,max}$, which results in a minimum turning radius constraint. Note that Eq. (2) ensures the superiority of the target in terms of both speed and maneuverability.

To facilitate the analytical derivation, the following common assumptions are adopted [21]: For the feasibility of the interception problem, the target is considered nonthreatening if it runs out of the lateral boundaries that one defined by the maximum heading angle variation $\Delta\theta_{T,\max}$, as shown in Fig. 2. Otherwise, the target can always escape with speed and maneuverability advantages over a long relative range unless a perfectly encircled formation can be established [31].

### 2.2. Kinematics equations of relative motion

The relative motion between the target and the $i$th missile can be represented based on a reference frame with the origin fixed at the target [32–34], which is denoted as $X_R - O_R - Y_R$. Then, the relative velocity is denoted by $V_{R_i}$ and defined as $V_{R_i} = V_{M_i} - V_T$, as shown in Fig. 3.

The corresponding heading angle is denoted by $\theta_R$. Hence, the following equations of motion in the prescribed reference frame can be derived:

$$\begin{cases} \dot{x} = V_R \cos\theta_R \\ \dot{y} = V_R \sin\theta_R \\ \dot{\theta}_R = \dfrac{a_R}{V_R} \\ \dot{\lambda} = -\dfrac{V_R}{r}\sin(\theta_R - \lambda) \end{cases} \tag{3}$$

The magnitude and heading angle of the relative velocity can be obtained as:

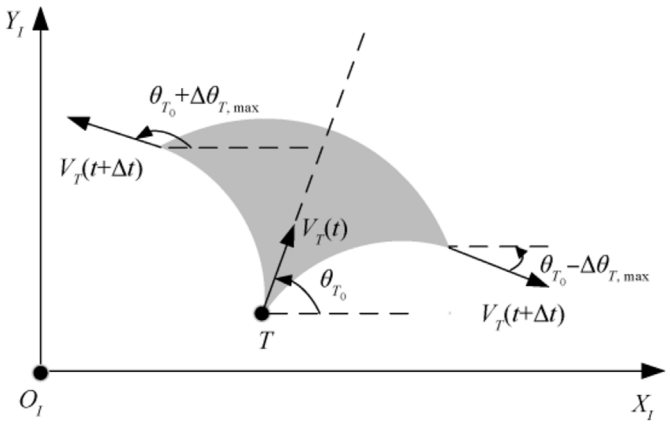


**Fig. 2.** Restricted escape zone of the target.

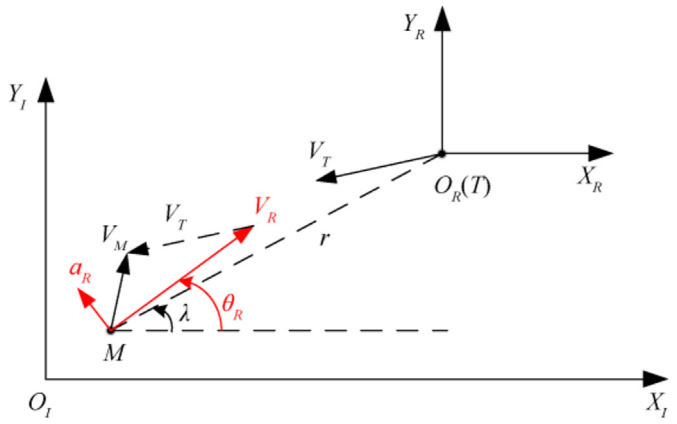


**Fig. 3.** Engagement geometry in the relative coordinate system.

$$V_R = V_M\sqrt{1+\rho^2-2\rho\cos(\theta_M-\theta_T)} \tag{4}$$

$$\theta_R = \arctan\frac{\sin\theta_M-\rho\sin\theta_T}{\cos\theta_M-\rho\cos\theta_T} \tag{5}$$

where $\rho>1$ is the speed ratio and is equal to $V_T/V_M$. The relative acceleration perpendicular to the relative velocity is denoted by $a_R$ and is equal to:

$$a_R = \cos(\theta_M-\theta_R)a_M - \cos(\theta_T-\theta_R)a_T \tag{6}$$

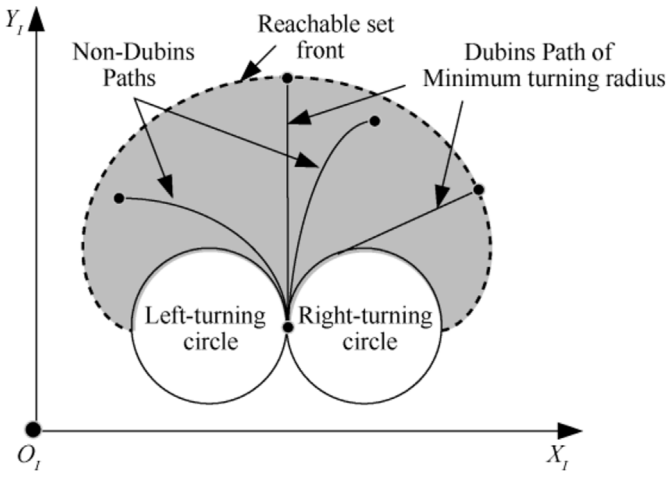


**Fig. 4.** Reachable set with the minimum turning radius.

where $\boldsymbol{u_i}(t,t+\Delta t)$ is the continuous control over the time range $[t,t+\Delta t]$ and $\varnothing$ represents all possible control inputs satisfying the relevant constraints.

Consequently, the equal-time line (ETL) is developed based on both sides' reachable sets of positions, which is a barrier that both sides' players can reach simultaneously following the shortest path via the minimum-time guidance [35]. The ETL can be achieved via Eq. (9) and is illustrated in Fig. 5.

$$ETL_i(t)=\{(x,y)\,|\,g(V_{M_i},a_{M_i,\max},\boldsymbol{x}_{M_i}(t),\Delta t)=g(V_T,a_{T,\max},\boldsymbol{x}_T(t),\Delta t),\Delta t\geq t_{EIT,i}\} \tag{9}$$

### 2.3. Analysis of conditions for successful interception

From the perspective of reachability, if all the positions that the target can reach over a certain period can also be reached by missiles, then successful interception is feasible. Under a near head-on or tail-chase engagement scenario, the kinematics can be linearized [20], and the resulting necessary condition for interception can be defined as the zero-effort miss (ZEM) distribution that falls inside the missile's maximum lateral displacement envelope. This traditional necessary condition is given by:

$$|ZEM_{M_i}|\leq a_{M_i,\max}t_{go,i}^2\Big/2 \tag{7}$$

However, when confronted with long time-to-go and drastic maneuvers, the assumption for the linearization of engagement kinematics, along with the traditional necessary conditions for interception, will be invalid [21]. Therefore, a reachability-based situation assessment is adopted to analyze the feasibility of the interception under nonlinear kinematics.

The reachable set is defined as all the states that can be reached from initial state $\boldsymbol{x}_i(t)=(x_i,y_i,\theta_i)^{\mathrm{T}}$ during a certain period $\Delta t$, which is described in Fig. 4 and expressed in the following equations:

$$RS_i(t,t+\Delta t|\boldsymbol{x}_i(t))=\{\boldsymbol{x}_i(t+\Delta t)|\forall\boldsymbol{u_i}(t,t+\Delta t)\in\varnothing\} \tag{8}$$

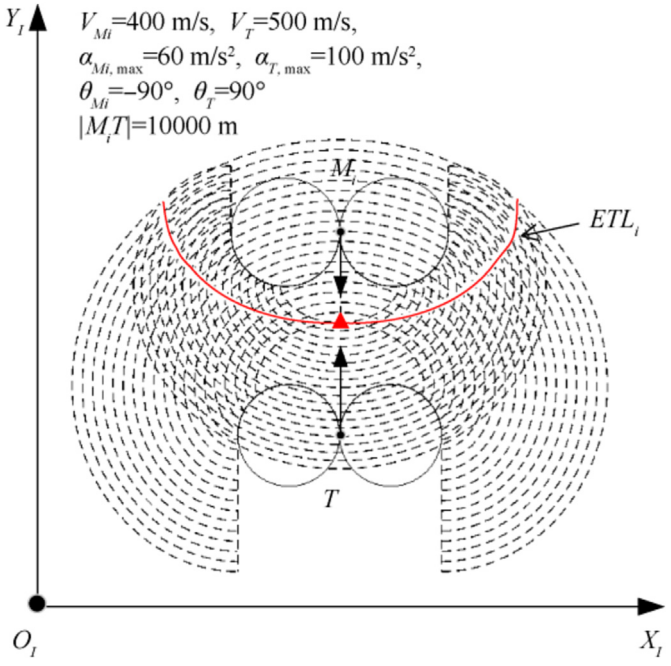


**Fig. 5.** The ETL that both sides can reach simultaneously.

where $g$ denotes the calculation function of the reachable set front (RSF) of the position, which theoretically equals the involute formula, and $t_{EIT,i}$ denotes the earliest intercept time, i.e., the reachable sets with respect to $t_{EIT,i}$ of both sides are tangent to each other.

The ETL can be regarded as a credible barrier for estimating intercept performance, which divides the engagement zone into two subzones. The target can reach any position within the subzone close to it earlier than the missile, which implies a foreseeable interception failure within the subzone. The opposite is true for the subzone close to the missile.

A necessary condition for a multi-on-one interception scenario under nonlinear kinematics can be satisfied by rational design of the engagement geometry. In such an engagement geometry, the ETLs are linked as described by Eq. (10) and Fig. 6, which allows the union of the missile reachable sets to cover the entire target escape zone, that is,

$$RSF_T(t, t+\Delta t|\boldsymbol{x}_T(t)) \backslash \bigcup_{i=1}^{n} RS_{M_i}(t, t+\Delta t|\boldsymbol{x}_{M_i}(t)) = \varnothing \tag{10}$$

From the perspective of zero-effort miss (ZEM), if a collision triangle can be constructed closely near or at impact, then successful interception can be guaranteed. In the reference frame of the relative motion, constructing a collision triangle implies that the relative velocity vector coincide with the LOS, i.e., $\theta_R = \lambda$.

Based on the above analysis, the authors are interested in the following two problems:

(1) The existing guidance strategy, which is based on the coverage of the reachable set of positions, is derived mainly for situations with a single moment. The coverage performance may degrade as the engagement progresses. Therefore, we are interested in investigating how to improve the dynamic coverage performance while the target is moving.
(2) To improve the dynamic coverage of the reachable set, how can the formation and maintenance of the collision triangle near impact be further improved?

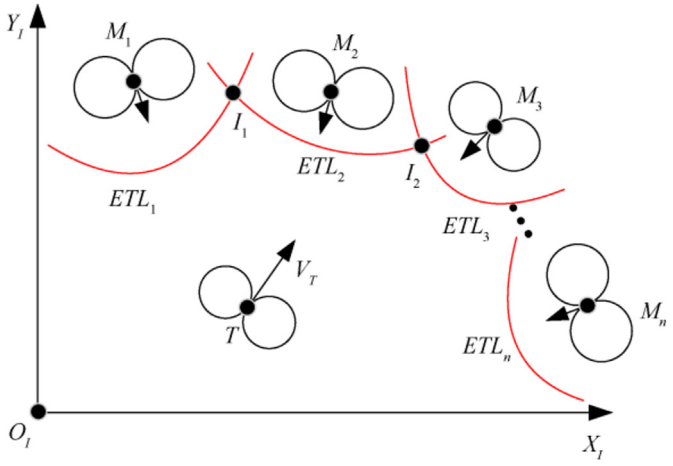


**Fig. 6.** The desired union intercept line.

## 3. Cooperative guidance strategy based on the maintenance of coverage and collision situation

To address and solve the above problems, a two-stage guidance strategy is developed in this section. The key involves designing a cooperative guidance strategy to coordinate multiple missile reachable sets to cover the virtual targets distributed on the RSF of the target, whereas impact angle constraints are imposed and optimized to improve the formation and maintenance of the collision triangle.

### 3.1. Virtual target analysis and selection

From the perspective of target movement, the virtual target $T_{V,i}$ characterize the probability distribution of the real target's position at impact, which can be regarded as the predicted interception points and are directly related to the target's maneuvering direction and magnitude [36,37]. From the perspective of the cooperative interception, the virtual target $T_{V,i}$ can be regarded as each missile's object of pursuit, which quantitatively decomposes and allocates the challenging intercept mission in the spatial dimension, as shown in Fig. 7 [19,20].

On the one hand, the virtual targets must satisfy asymptotic consistency in terms of time and position. When the time-to-go approaches zero, the virtual targets and the real target must

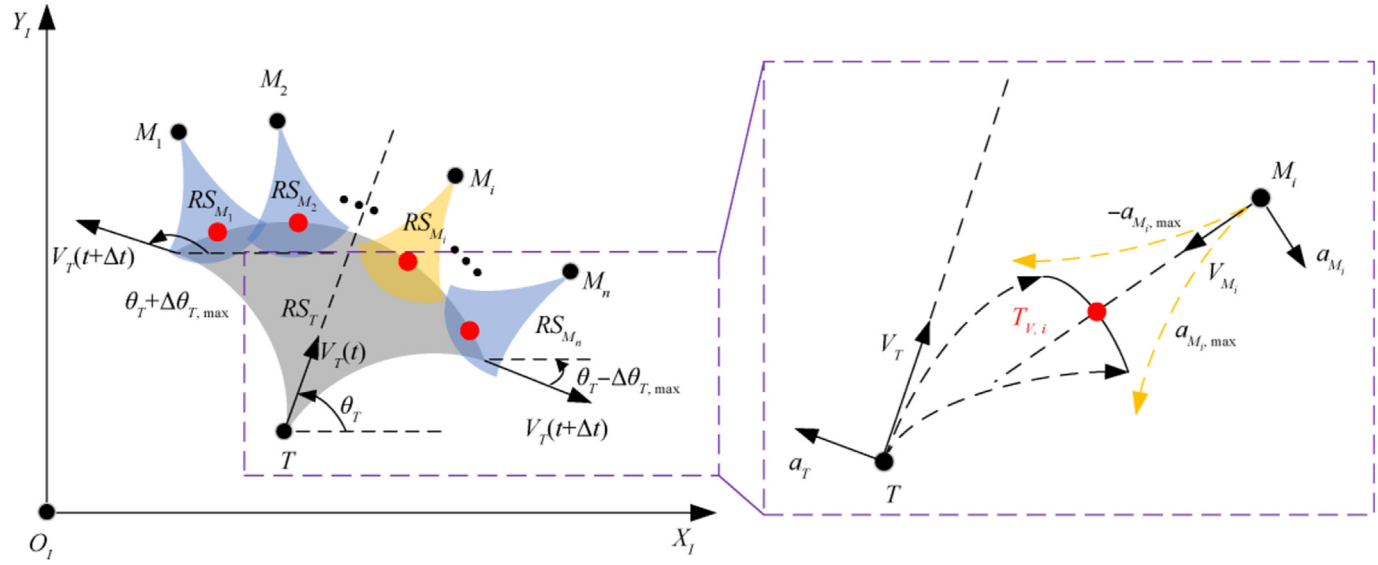


**Fig. 7.** Schematic of the terminal engagement states of cooperative interception.

coincide. On the other hand, the virtual targets should characterize the typical maneuvering direction and magnitude. In this way, the rational use of multiple missiles to pursue their respective virtual targets can better cope with the target's unknown maneuvering strategy. Therefore, the problem of covering the target's reachable set of positions can be transferred to pursue multiple virtual targets.

The virtual targets for each missile are selected from the real target's RSF of the position, which represents the furthest position that can be reached by the target through different maneuver directions and magnitudes. The RSF of the position of the player $i$, denoted by $RSF_i$, is computed as follows:

$$RSF_i(t, t+\Delta t|\boldsymbol{x}_i(t)) = g(V_i, a_{i,\max}, \boldsymbol{x}_i(t), \Delta t) = RSF_{i,R} \cup RSF_{i,L} \tag{11}$$

where $RSF_{i,R}$ and $RSF_{i,L}$ denote the right and left halves of $RSF_i$, respectively, with respect to the heading direction, which can be obtained via the involute formula as follows:

$$P_{T_{V,i}} = \begin{cases} \begin{pmatrix} x_{O_{T,R}} + r_{O_T}\left[-\sin\left(\theta_T - \varphi_{T_{V,i}}\right) + \varphi_{T_{V,i}}\cos\left(\theta_T - \varphi_{T_{V,i}}\right)\right] \\ y_{O_{T,R}} + r_{O_T}\left[-\cos\left(\theta_T - \varphi_{T_{V,i}}\right) + \varphi_{T_{V,i}}\sin\left(\theta_T - \varphi_{T_{V,i}}\right)\right] \end{pmatrix}^{\mathrm{T}} & i \le \dfrac{n+1}{2} \\ \begin{pmatrix} x_{O_{T,L}} + r_{O_T}\left[\sin\left(\theta_T + \varphi_{T_{V,i}}\right) - \varphi_{T_{V,i}}\cos\left(\theta_T + \varphi_{T_{V,i}}\right)\right] \\ y_{O_{T,L}} + r_{O_T}\left[-\cos\left(\theta_T + \varphi_{T_{V,i}}\right) + \varphi_{T_{V,i}}\sin\left(\theta_T + \varphi_{T_{V,i}}\right)\right] \end{pmatrix}^{\mathrm{T}} & i > \dfrac{n+1}{2} \end{cases} \tag{15}$$

$$RSF_{i,R} = \left\{(x,y)\middle| x = x_{O_{i,R}} + r_{O_i}[-\sin(\theta_i - \varphi) + \varphi\cos(\theta_i - \varphi)], \right.$$
$$\left. y = y_{O_{i,R}} + r_{O_i}[-\cos(\theta_i - \varphi) + \varphi\sin(\theta_i - \varphi)], \varphi \in \left[0, \frac{V_i \Delta t}{r_{O_i}}\right]\right\} \tag{12}$$

$$RSF_{i,L} = \left\{(x,y)\middle| x = x_{O_{i,L}} + r_{O_i}[\sin(\theta_i + \varphi) - \varphi\cos(\theta_i + \varphi)], \right.$$
$$\left. y = y_{O_{i,L}} + r_{O_i}[-\cos(\theta_i + \varphi) + \varphi\sin(\theta_i + \varphi)], \varphi \in \left[0, \frac{V_i \Delta t}{r_{O_i}}\right]\right\} \tag{13}$$

where $\theta_i$ denotes the heading angle; $(x_{O_{i,R}}, y_{O_{i,R}})$ and $(x_{O_{i,L}}, y_{O_{i,L}})$ denote the coordinates of the centers of the right- and left-turning circles of player $i$, which are equal to $(x_i + r_{O_i}\sin\theta_i, y_i - r_{O_i}\cos\theta_i)$ and $(x_i - r_{O_i}\sin\theta_i, y_i + r_{O_i}\cos\theta_i)$, respectively; and $r_{O_i}$ denotes the minimum turning radius, which is equal to $V_i^2/a_{i,\max}$.

To ensure that the intercepting missiles surround the real target and gradually approach it during the process of pursuing the virtual targets, it is crucial to determine the $\Delta t$ term in Eq. (11) and the selection method of virtual targets on the RSF. The reachable set of positions shrinks as the time-to-go decreases and converges to the real target when the time-to-go approaches zero. The time-to-go term is adopted as the $\Delta t$ term for the RSF calculations. For PN or its variants, the time-to-go for the engagement between the maneuvering target and the $i$th missile is commonly estimated as follows [38]:

$$t_{go,i} = \frac{r_i}{V_{M,i}}\left[1 + \frac{\theta_i^2}{2(2N-1)}\right] \tag{14}$$

where $N$ is the navigation gain.

To ensure virtual target characterization for the real target motion under various maneuvering directions and magnitudes, virtual targets are selected according to the heading angle variation. The sign and magnitude of the target's heading angle variation correspond to the target's maneuver direction and magnitude, respectively. For targets with unknown maneuvering strategies, arbitrary maneuvering directions and magnitudes within their capabilities are feasible. To address the unknown distribution of the maneuver direction and magnitude of a target, it is reasonable to evenly select virtual targets on the real target's RSF with respect to its heading angle variation. The virtual target geometry is depicted in Fig. 8, where $\varphi_{T_{V,i}}$ represents the deflection angle of the virtual target from the real target. Therefore, the $\eta$ virtual targets for the $\eta$ intercepting missiles are selected as follows:

where $\varphi_{T_{V,i}}$ is equal to

$$\varphi_{T_{V,i}} = \begin{cases} \left(\dfrac{n+1}{2} - i\right)\dfrac{\Delta\theta_{T,\max}}{n-1} + \theta_T & \Delta\theta_{T,\max} \le \dfrac{V_T t_{go,i}}{r_{O_i}} \\ \left(\dfrac{n+1}{2} - i\right)\dfrac{1}{n-1}\dfrac{V_T t_{go,i}}{r_{O_i}} + \theta_T & \Delta\theta_{T,\max} > \dfrac{V_T t_{go,i}}{r_{O_i}} \end{cases} \tag{16}$$

where $\Delta\theta_{T,\max}$ represents the upper limit of the accumulative

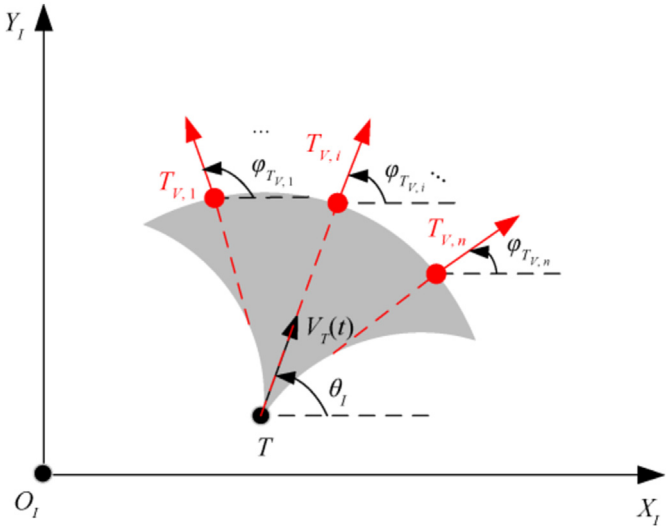


**Fig. 8.** Virtual target geometry schematic.

heading angle variation of the target.

### 3.2. Optimizing angle constraints for pursuing virtual targets

To improve the formation and maintenance of the collision triangle near impact, the impact angle needs to be controlled to pursue virtual targets. Hence, we are interested in what impact angle is beneficial for the missiles to win the contest against the target in terms of relative velocity control. In other words, the ideal shape of the collision triangle for the intercepting missile should be analyzed, which is further related to the impact angle constraints.

According to Eq. (5), the relative heading angle rate $\dot{\theta}_R$ can be obtained as follows:

$$\dot{\theta}_R = \frac{1}{1+\left(\frac{\sin\theta_M - \rho\sin\theta_T}{\cos\theta_M - \rho\cos\theta_T}\right)^2} \cdot \frac{\dot{\theta}_M - \rho\cos(\theta_M-\theta)_T\dot{\theta}_M - \rho\cos(\theta_M-\theta)_T\dot{\theta}_T + \rho^2\dot{\theta}_T}{(\cos\theta_M - \rho\cos\theta_T)^2} \tag{17}$$

For ease of computation, the expression for $\dot{\theta}_R$ can be further reduced to:

$$\dot{\theta}_R = \frac{HL}{W^2}\left(\frac{1}{H}\dot{\theta}_M + \frac{\rho}{L}\dot{\theta}_T\right) \tag{18}$$

where $H = \rho - \cos(\theta_M - \theta_T)$, $L = 1 - \rho\cos(\theta_M - \theta_T)$ and $W = \sqrt{1+\rho^2-2\rho\cos(\theta_M-\theta_T)}$.

To compare the influence of both sides' heading angles on the relative velocity direction variation, Eq. (18) is differentiated with respect to $\dot{\theta}_M$ and $\dot{\theta}_T$, respectively, as follows:

$$\frac{\partial\dot{\theta}_R}{\partial\dot{\theta}_M} = \frac{1-\rho\cos(\theta_M-\theta_T)}{1+\rho^2-2\rho\cos(\theta_M-\theta_T)} \tag{19}$$

$$\frac{\partial\dot{\theta}_R}{\partial\dot{\theta}_T} = \frac{\rho[\rho-\cos(\theta_M-\theta_T)]}{1+\rho^2-2\rho\cos(\theta_M-\theta_T)} \tag{20}$$

Note that it is impossible for missiles to intercept a superior target in some scenarios, such as tail-chase scenarios. Therefore, the entire value range of $(\theta_M - \theta_T)$ is not worth investigating, only head-on and lateral engagement scenarios need to be considered when $V_M < V_T$, so the considerable value range is restricted to:

$$\theta_M - \theta_T \in \left(-\frac{3}{2}\pi, -\frac{1}{2}\pi\right) \cup \left(\frac{1}{2}\pi, \frac{3}{2}\pi\right) \tag{21}$$

Considering that $\rho > 1$, it follows from Eqs. (19)–(21) that,

$$\begin{cases} \cos(\theta_M-\theta_T) < 0 \\ 1-\rho\cos(\theta_M-\theta_T) > 0 \\ \rho - \cos(\theta_M-\theta_T) > 0 \\ 1+\rho^2-2\rho\cos(\theta_M-\theta_T) > 0 \end{cases} \tag{22}$$

According to Eq. (22), one can readily derive the following:

$$\begin{cases} \left|\frac{\partial\dot{\theta}_R}{\partial\dot{\theta}_M}\right| = \frac{\partial\dot{\theta}_R}{\partial\dot{\theta}_M} \\ \left|\frac{\partial\dot{\theta}_R}{\partial\dot{\theta}_T}\right| = \frac{\partial\dot{\theta}_R}{\partial\dot{\theta}_T} \end{cases} \tag{23}$$

The ideal collision triangle should maximize the value of $\left|\frac{\partial\dot{\theta}_R}{\partial\dot{\theta}_M}\right|$, while minimizing the value of $\left|\frac{\partial\dot{\theta}_R}{\partial\dot{\theta}_T}\right|$. In this case, the missile's velocity vector has the greatest effect on the relative velocity vector and the target's velocity vector has the least effect on the relative velocity vector, which is favorable for the missile side in terms of controlling the relative velocity vector and the maintaining the collision triangle. From this perspective, setting $u = \theta_M - \theta_T$ and further differentiating Eqs. (19) and (20), results in:

$$\frac{\partial}{\partial u}\left|\frac{\partial\dot{\theta}_R}{\partial\dot{\theta}_M}\right| = \frac{\rho(\rho^2-1)\sin u}{(1+\rho^2-2\rho\cos u)^2} \tag{24}$$

$$\frac{\partial}{\partial u}\left|\frac{\partial\dot{\theta}_R}{\partial\dot{\theta}_T}\right| = -\frac{\rho(\rho^2-1)\sin u}{(1+\rho^2-2\rho\cos u)^2} \tag{25}$$

Consequently, the extrema of $\left|\frac{\partial\dot{\theta}_R}{\partial\dot{\theta}_M}\right|$ and $\left|\frac{\partial\dot{\theta}_R}{\partial\dot{\theta}_T}\right|$ are computed as follows:

$$\left|\frac{\partial\dot{\theta}_R}{\partial\dot{\theta}_M}\right|_{\max} = \left.\frac{1-\rho\cos(\theta_M-\theta_T)}{1+\rho^2-2\rho\cos(\theta_M-\theta_T)}\right|_{\theta_M-\theta_T=\pm\pi} = \frac{1+\rho}{1+\rho^2+2\rho} = \frac{1}{1+\rho} \tag{26}$$

$$\left|\frac{\partial\dot{\theta}_R}{\partial\dot{\theta}_T}\right|_{\min} = \left.\frac{\rho[\rho-\cos(\theta_M-\theta_T)]}{1+\rho^2-2\rho\cos(\theta_M-\theta_T)}\right|_{\theta_M-\theta_T=\pm\pi} = \frac{\rho(\rho+1)}{1+\rho^2+2\rho} = \frac{\rho}{1+\rho} \tag{27}$$

According to Eqs. (26) and (27), the ideal engagement geometry is a head-on collision course. The corresponding impact angle for pursuing the virtual target is $\pi$ or $-\pi$. Moreover, this impact angle is also beneficial for improving the coverage performance of the target's position reachable set, since the position diversion envelope of each missile is fully used to cover the RSF of the target's position, as shown in Fig. 9.

### 3.3. Cooperative guidance strategy

A two-stage cooperative guidance law is proposed on the basis of the virtual targets and the relative kinematics. The first stage is conducted by an impact angle control guidance law to improve the coverage performance of the target's position reachable set and the maintenance of the collision course, whereas the second stage focuses on intercepting the highly maneuvering target.

The impact angle control guidance law in Ref. [33] is adopted in the first stage for pursuing the moving virtual targets, and the

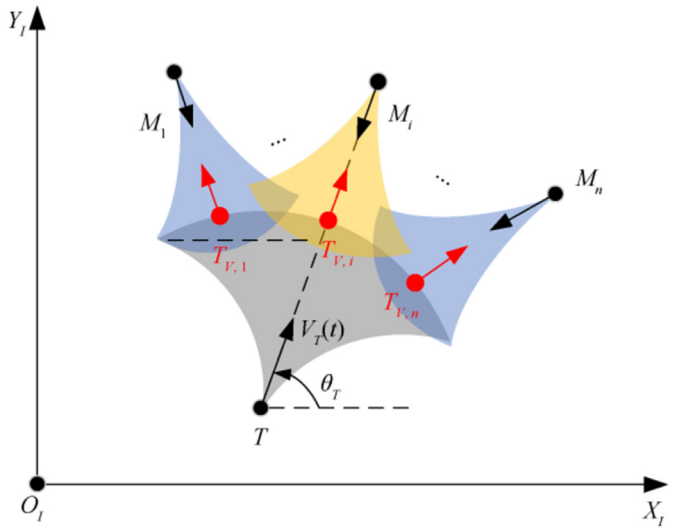


**Fig. 9.** The coverage situation of pursuing virtual targets.

command in the reference frame can be expressed as follows:

$$a_{R_i} = N_1 V_{R_i} \dot{\lambda}_i + \frac{N_2(N_1-1)V_{R_i}\dot{r}_i}{r}\varepsilon \tag{28}$$

where $\varepsilon$ represents the predicted angle error at the terminal time, and $N_1$ and $N_2$ denote the guidance gains.

Furthermore, substituting Eq. (28) into Eq. (6) yields the guidance command of the missile as:

$$a_{M_i} = \frac{a_{R_i}}{\cos(\theta_{M_i}-\theta_{R_i})} + \frac{\cos(\theta_T-\theta_{R_i})}{\cos(\theta_{M_i}-\theta_{R_i})}a_T \tag{29}$$

With the predetermined impact angle constraint, all the missiles are capable of covering the RSF of the target's position effectively.

Owing to the target's high speed and maneuverability, $a_{M_i}$ may become saturated at certain times, i.e., the acceleration command required to satisfy Eq. (29) exceeds $a_{M_i,\max}$. When this situation persists, the maneuvers of missiles can no longer meet the demand to maintain coverage performance. Therefore, it is necessary to switch guidance laws based on the current position reachable set.

The position reachable set analysis is based on the shortest Dubins paths. For the effectiveness of the interception situation constructed based on the coverage strategy of the reachable set, the terminal intercept trajectory should be analogous to that of the Dubins trajectory [39]. Motivated by the differential game guidance law that is proposed in Refs. [10,20], the following guidance law is adopted for the second guidance stage, namely,

$$a_{M_i} = a_{M_i,\max}\text{sign}(ZEM_i^*) \tag{30}$$

where the $ZEM_i^*$ is defined in the reference frame of relative motion and is equal to the minimum distance when the relative distance point passes the origin with zero effort control in the reference frame of relative motion, which avoids the model linearization process [40]. $ZEM_i^*$ is calculated via Eq. (31) and described in Fig. 10.

$$ZEM_i^* = -r_i \sin(\theta_{R_i}-\lambda_i) \tag{31}$$

Consequently, the final form of the guidance law can be expressed as:

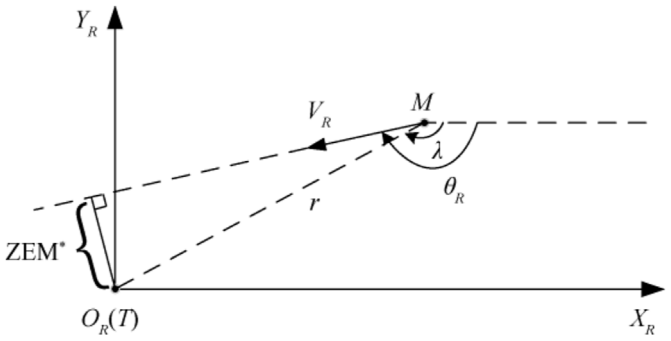


**Fig. 10.** Zero effort miss in the relative coordinate system.

$$a_{M_i} = \begin{cases} \dfrac{a_{R_i}}{\cos(\theta_{M_i}-\theta_{R_i})} + \dfrac{\cos(\theta_T-\theta_{R_i})}{\cos(\theta_{M_i}-\theta_{R_i})}a_T & \text{stage 1} \\ a_{M_i,\max}\text{sign}(ZEM_i^*) & \text{stage 2} \end{cases} \tag{32}$$

when the missile's acceleration continuously saturates, the guidance law switches to the second guidance stage.

In this case, the process of the two-stage cooperative guidance strategy is shown in Fig. 11.

## 4. Simulations and analysis

### 4.1. Simulation setup

To assess the performance of the proposed guidance strategy, comparisons with existing guidance strategies are conducted for the same initial engagement geometry. The simulations involve

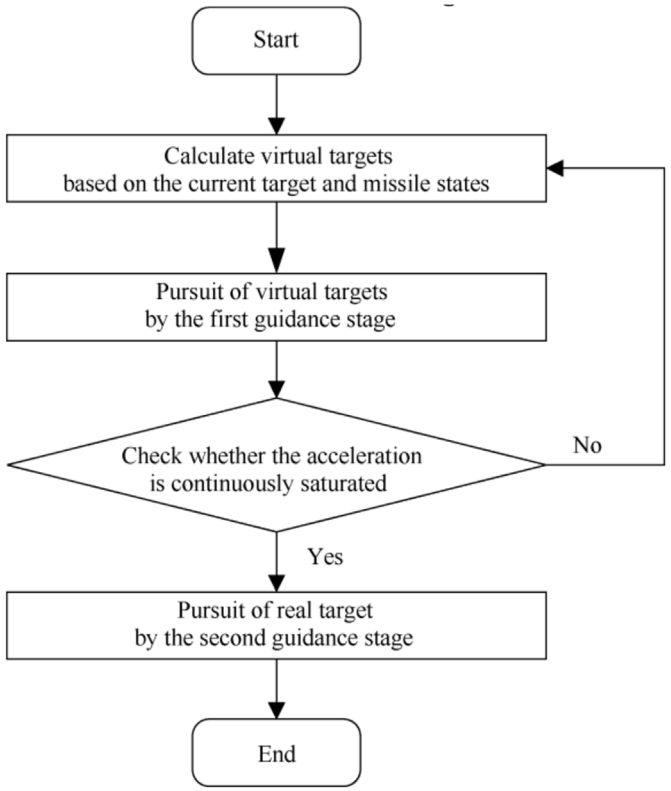


**Fig. 11.** Process of the two-stage cooperative guidance strategy.

three intercepting missiles, denoted by $M_1$, $M_2$, and $M_3$. All intercepting missiles travel at a constant speed of 400 m/s with a maximum acceleration limit of 60 m/s$^2$, whereas the target travels with a superior speed of 500 m/s and maneuverability of 100 m/s$^2$. The target is positioned at (0,0) m with a heading angle of 90°. The initial position of the median missile $M_2$ is (0,10000) m with a heading angle of −90°. In order to satisfy the necessary condition of the interception in Eq. (10), an initial formation based on reachable set analysis is adopted, as shown in Eqs. (33) and (34) [21]. Therefore, the missiles $M_1$ and $M_3$ are positioned at (−7910.3,10337.0) m and (7910.3,10337.0) m with heading angles of −50° and −130°, respectively. The maximum detection distance of the target is $r_d = 6000$. The target can detect intercepting missiles and maneuver to avoid them when the relative distance satisfies $r_i > r_d$. The upper limit of the accumulative heading angle variation of the target is set to $\Delta\theta_{T,\max} = 80°$. The guidance gains of the first stage guidance law in Eq. (26) are set to $N_1 = 3$ and $N_2 = 2$. The simulation step is set to 0.001 s. When the missile's acceleration saturates for 10 consecutive steps, the guidance strategy switches to the second guidance stage. The autopilot is assumed to have a first-order lag with a time constant of 0.2 s. Considering the damage radius, successful interception is achieved when the miss distance is less than 10 m. The calculation time to generate one guidance command by the proposed method is approximately 50 ms with a 4.0 GHz quad-core processor and 16 GB of RAM.

$$\begin{cases} P_{M_i}(t_0) = P_T\left(t_0 + \left(\frac{n+1}{2} - i\right)\Delta t_C\right) + \boldsymbol{v}_T\left(t_0 + \left(\frac{n+1}{2} - i\right)\Delta t_C\right)\left[r_{\frac{n+1}{2}}(t_0) + \left(\frac{n+1}{2} - i\right)V_M\Delta t_C\right] \\ \boldsymbol{v}_T\left(t_0 + \left(\frac{n+1}{2} - i\right)\Delta t_C\right) = \begin{pmatrix} \cos\left(\theta_T + \left(\frac{n+1}{2} - i\right)\Delta\theta_{T_C}\right) \\ \sin\left(\theta_T + \left(\frac{n+1}{2} - i\right)\Delta\theta_{T_C}\right) \end{pmatrix}^{\mathrm{T}} \\ P_T\left(t_0 + \left(\frac{n+1}{2} - i\right)\Delta t_C\right) = \begin{pmatrix} x_{O_{T,L}} + r_{O_T}\sin\left[\theta_T + \left(\frac{n+1}{2} - i\right)\Delta\theta_{T_C}\right] \\ y_{O_{T,L}} - r_{O_T}\cos\left[\theta_T + \left(\frac{n+1}{2} - i\right)\Delta\theta_{T_C}\right] \end{pmatrix}^{\mathrm{T}} \\ \theta_{M_i}(t_0) = \theta_T + \left(\frac{n+1}{2} - i\right)\Delta\theta_{T_C} - \pi \end{cases} \tag{33}$$

$$\begin{cases} P_{M_i}(t_0) = P_T\left(t_0 + \left(i - \frac{n+1}{2}\right)\Delta t_C\right) + \boldsymbol{v}_T\left(t_0 + \left(i - \frac{n+1}{2}\right)\Delta t_C\right)\left[r_{\frac{n+1}{2}}(t_0) + \left(i - \frac{n+1}{2}\right)V_M\Delta t_C\right] \\ \boldsymbol{v}_T\left(t_0 + \left(i - \frac{n+1}{2}\right)\Delta t_C\right) = \begin{pmatrix} \cos\left(\theta_T - \left(i - \frac{n+1}{2}\right)\Delta\theta_{T_C}\right) \\ \sin\left(\theta_T - \left(i - \frac{n+1}{2}\right)\Delta\theta_{T_C}\right) \end{pmatrix}^{\mathrm{T}} \\ P_T\left(t_0 + \left(i - \frac{n+1}{2}\right)\Delta t_C\right) = \begin{pmatrix} x_{O_{T,R}} - r_{O_T}\sin\left[\theta_T - \left(i - \frac{n+1}{2}\right)\Delta\theta_{T_C}\right] \\ y_{O_{T,R}} + r_{O_T}\cos\left[\theta_T - \left(i - \frac{n+1}{2}\right)\Delta\theta_{T_C}\right] \end{pmatrix}^{\mathrm{T}} \\ \theta_{M_i}(t_0) = \theta_T - \left(i - \frac{n+1}{2}\right)\Delta\theta_{T_C} - \pi \end{cases} \tag{34}$$

where $\boldsymbol{v}_T$ denotes the unit velocity vector of the target, $\Delta\theta_{T_C}$ is the coverage range for the target heading angle deviation by $M_{\frac{n+1}{n}}$ [21] and $\Delta t_C$ is the time spent by the target $T$ escaping the coverage of $M_i$ and is equal to:

$$\Delta t_C = \frac{V_T\Delta\theta_{T_C}}{a_{T,\max}} \tag{35}$$

For comparison, the simulation results of the reachability-based cooperative strategy (RCS) [21], coverage-based cooperative guidance (CBCG) [22] and APN are also presented and the guidance strategies are expressed as follows:

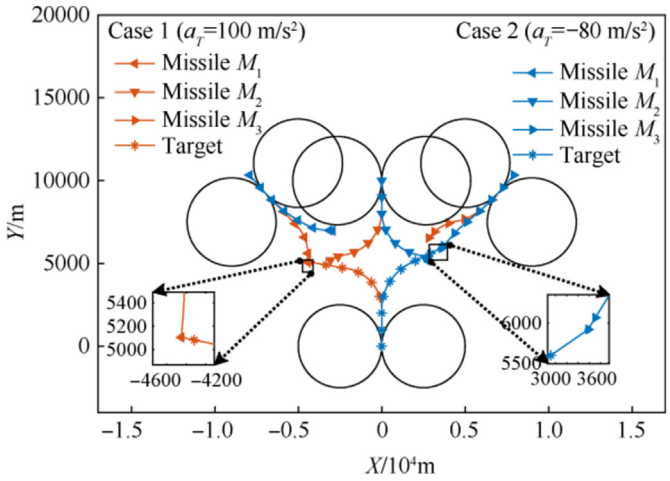


**Fig. 12.** Cooperative guidance trajectories in Cases 1 and 2 via the SMCS.

$$
\begin{cases}
RCS: a_{M_i}(t) = \begin{cases} a_{M_i,\max}\operatorname{sign}(ZEM_i') & t \geq t_i \\ 0 & \text{otherwise} \end{cases} \\
t_i = \dfrac{V_T \Delta\theta_{T_C}\left| i - \dfrac{n+1}{2} \right|}{a_{T,\max}} + t_{T,man} \\
APN: a_{M_i}(t) = N\dfrac{ZEM_i(t)}{t_{go,i}^2} + \dfrac{N\hat{a}_t(t)}{2} \\
ZEM_i(t) = y_i(t) + \dot{y}_i(t)t_{go,i} + \dfrac{\hat{a}_t(t)t_{go,i}^2}{2} \\
CBCG: a_{M_i}(t) = N\left(V_{M_i}\dot{\lambda}_{M_i} - B_{M_i}\right) \\
B_{M_i} = -\dfrac{1}{2}a_{T,M_i,s}\cos\eta_{T,M_i f,s}
\end{cases}
\tag{36}
$$

where $ZEM_i'$ is defined by the ETL, $t_i$ is the trigger time and $t_{T,man}$ is the start time of the target maneuver [21]. The navigation gain is set

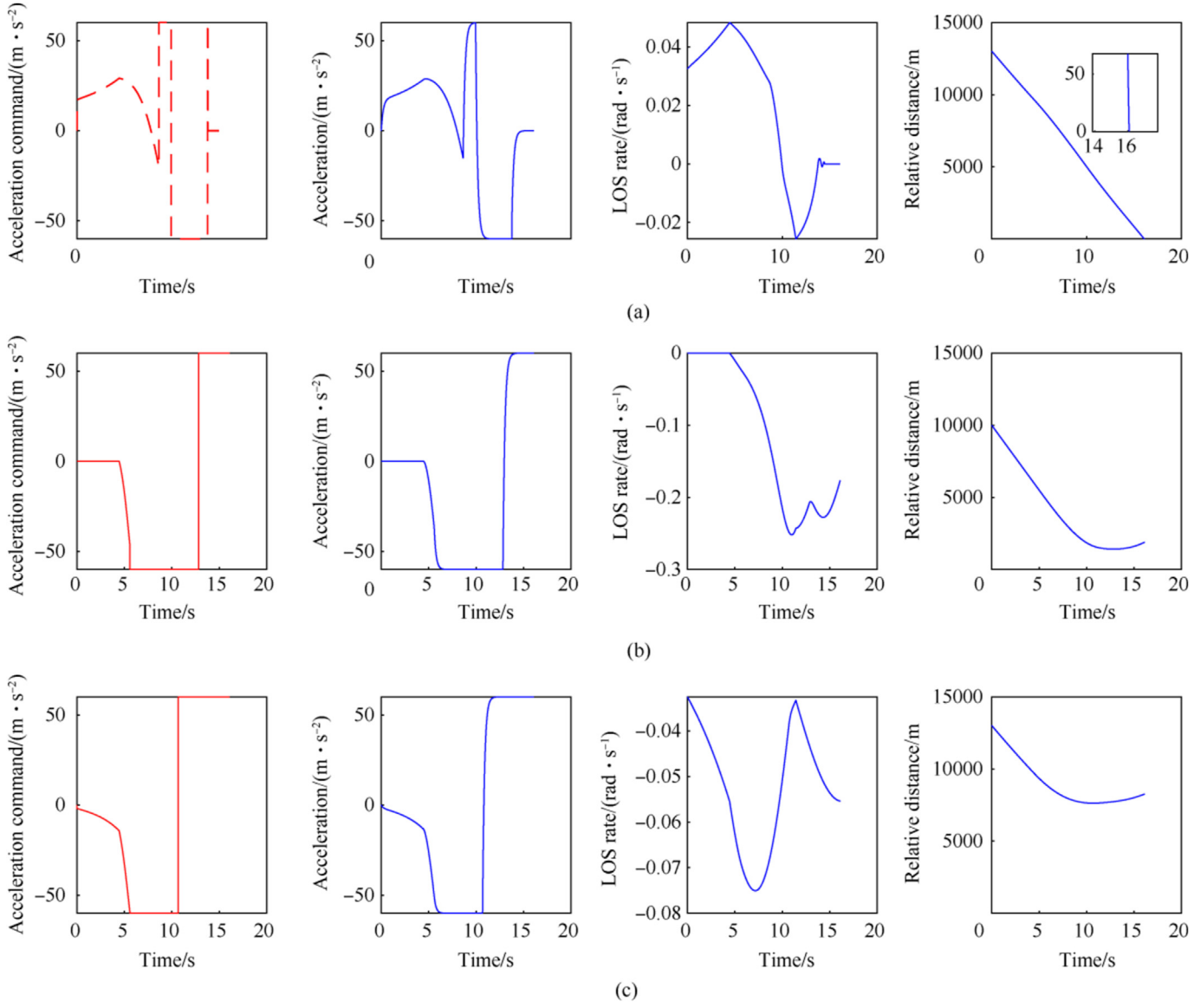


**Fig. 13.** Time history of commands, acceleration, LOS rate and relative distance of the missile team in Case 1: (a) Missile $M_1$; (b) Missile $M_2$; (c) Missile $M_3$.

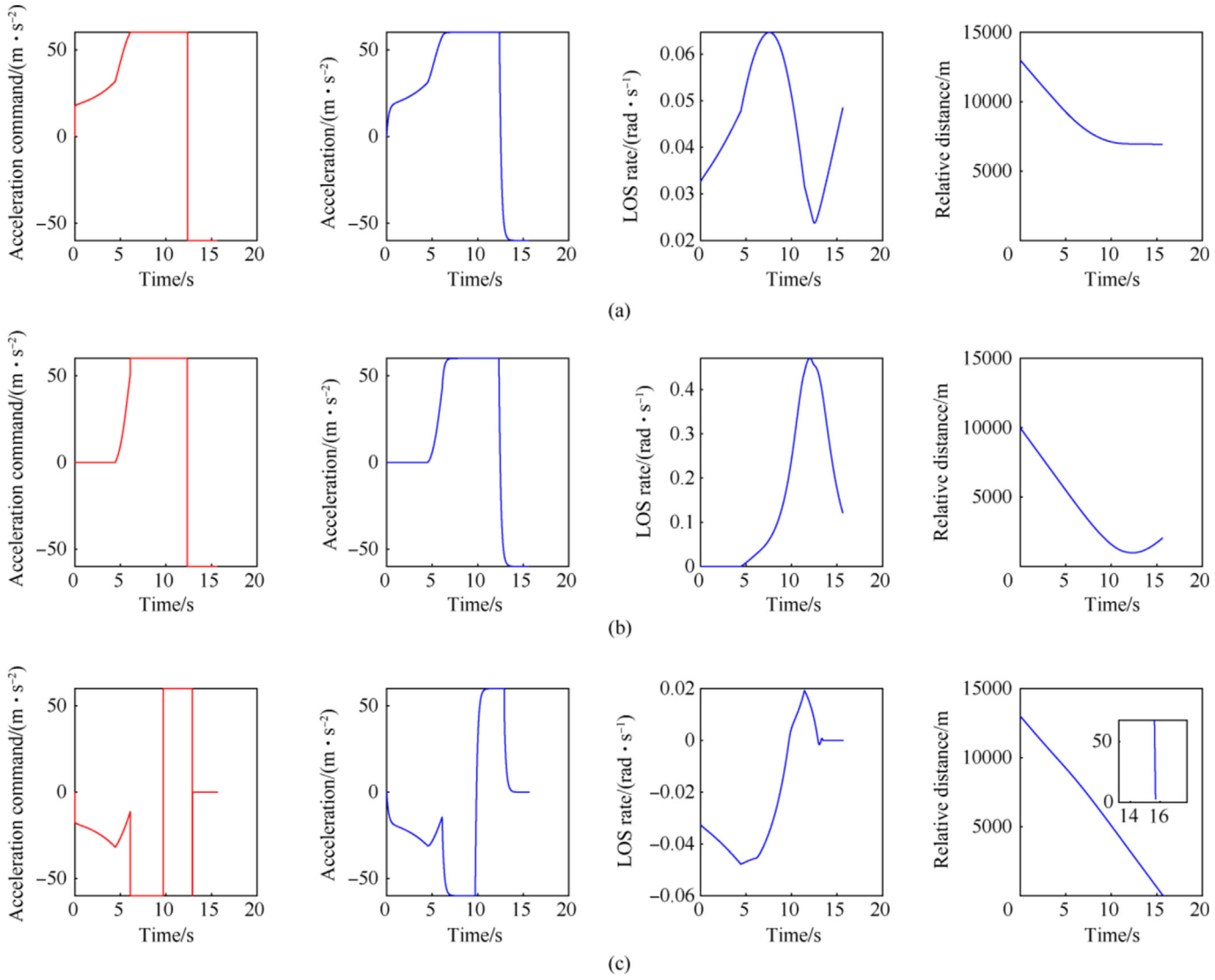


**Fig. 14.** Time history of commands, acceleration, LOS rate and relative distance of the missile team in Case 2: (a) Missile $M_1$; (b) Missile $M_2$; (c) Missile $M_3$.

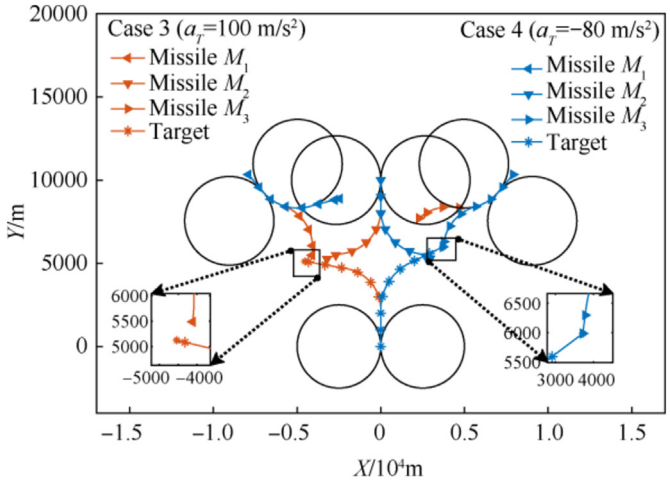


**Fig. 15.** Cooperative guidance trajectories in Cases 3 and 4 via the RCS.

to 3. $\hat{a}_t(t)$ is the estimated target acceleration, which is set to the ideal value, i.e. the true target acceleration. $y_i(t)$ is the normal distance to the LOS. $B_{M_i}$ is the bias term in the guidance command, which is calculated via standard ballistic trajectory parameters $a_{T,M_i,s}$ and $\eta_{T,M_i,f,s}$ [22].

### 4.2. Comparison to the other methods

First, assume that the target executes a constant maneuver as expressed in Eqs. (37) and (38), which are denoted by Case 1 and Case 2, respectively.

$$a_T = \begin{cases} 0 & r_i > r_d \\ 100\ \mathrm{m/s^2} & r_i \le r_d \text{ and } |\theta_T - \theta_{T_0}| \le \Delta\theta_{T,\max} \\ 0 & r_i \le r_d \text{ and } |\theta_T - \theta_{T_0}| > \Delta\theta_{T,\max} \end{cases} \tag{37}$$

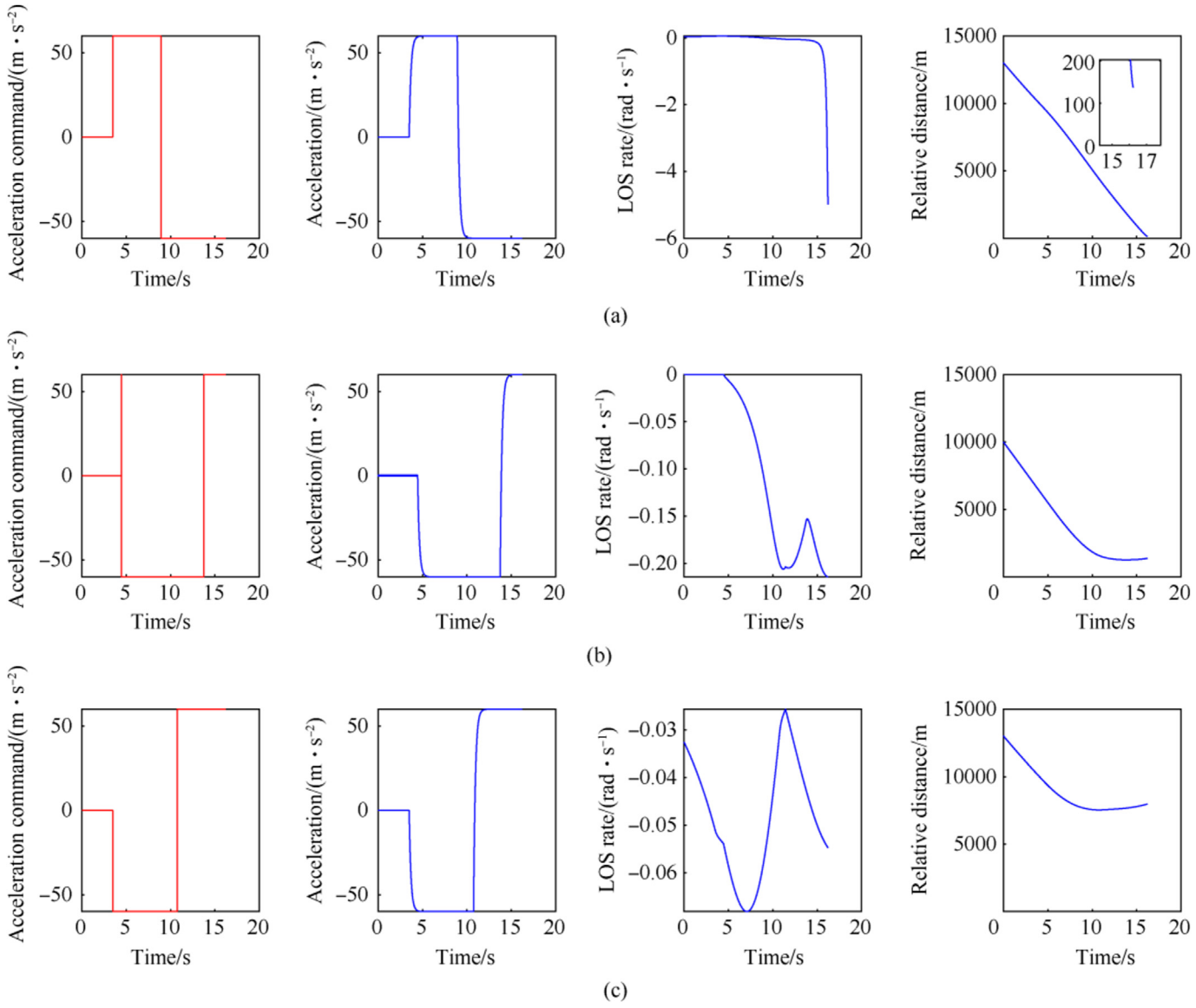


**Fig. 16.** Time history of commands, acceleration, LOS rate, and relative distance of the missile team in Case 3: (a) Missile $M_1$; (b) Missile $M_2$; (c) Missile $M_3$.

$$a_T = \begin{cases} 0 & r_i > r_d \\ -80\ \mathrm{m/s^2} & r_i \le r_d \text{ and } |\theta_T - \theta_{T_0}| \le \Delta\theta_{T,\max} \\ 0 & r_i \le r_d \text{ and } |\theta_T - \theta_{T_0}| > \Delta\theta_{T,\max} \end{cases} \tag{38}$$

Let the three missiles $M_1$, $M_2$, and $M_3$ adopt the proposed SMCS to intercept the target. Fig. 12 shows the flight trajectories of the three missiles and the target. Regardless of whether the target turns left or right, it will be successfully intercepted in the end. This is because the three intercepting missiles cover the target's maneuvering range and maintain this situation by pursuing the virtual targets. Figs. 13 and 14 show the time histories of the commands, acceleration, LOS rate and relative distance of the missile team in Cases 1 and 2, respectively. Meanwhile, the small window in the relative distance figure shows the miss distance at the final moment. It can be revealed that if the missile can successfully intercept the target, the corresponding value of the LOS rate changes smoothly and converges to zero gradually. The SMCS steers missile $M_1$ and missile $M_3$ to maintain the collision triangle near impact in Cases 1 and 2, respectively. According to the acceleration command variation, it can be seen that missile $M_3$ in Case 1 is continuously saturated with the acceleration command at $t = 5.58$ s, and missile $M_1$ in Case 2 is continuously saturated with the acceleration command at $t = 6.09$ s, which reflects the switching process of the guidance law, respectively.

In Cases 3–6, the intercept performance of RCS and CBCG is investigated. The initial conditions, including the missile formation and target maneuvering, in Cases 3 and 5 are the same as those in Case 1, and in Cases 4 and 6 are the same as those in Case 2, except that the guidance law is switched to RCS and CBCG, respectively. The corresponding trajectories of the missiles and target are plotted in Figs. 15 and 18, respectively, while Figs. 16, 17, 19, and 20 show the time histories of the commands, acceleration, LOS rate and relative distance of the missile team in Cases 3–6, respectively. It can be

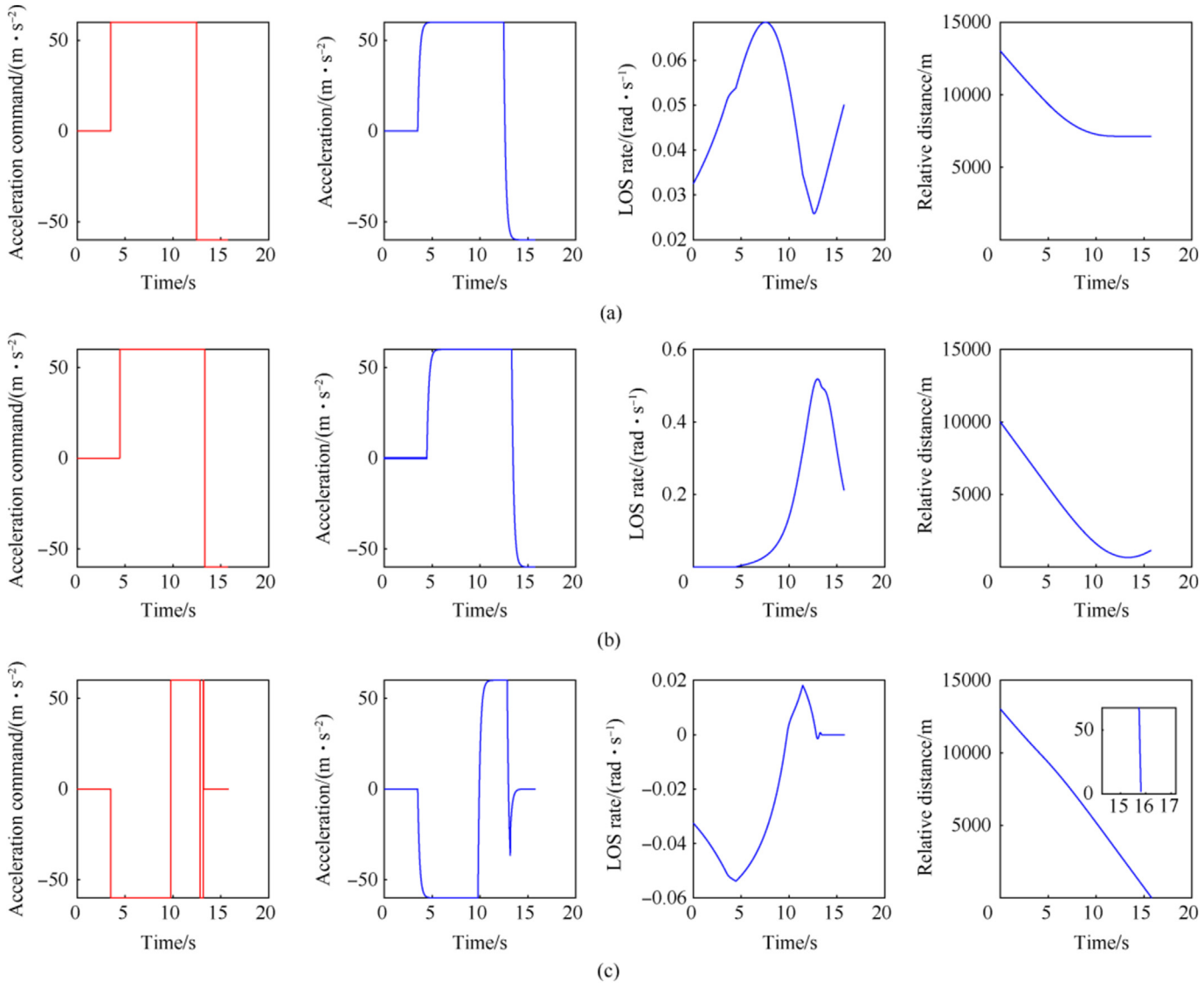


**Fig. 17.** Time history of commands, acceleration, LOS rate, and relative distance of the missile team in Case 4: (a) Missile $M_1$; (b) Missile $M_2$; (c) Missile $M_3$.

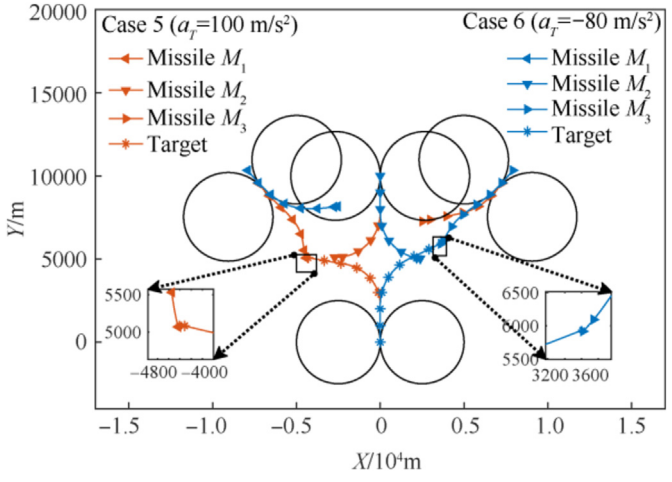


**Fig. 18.** Cooperative guidance trajectories in Cases 5 and 6 via the CBCG.

seen that in Cases 3, 5, and 6, although one missile in each case was able to gradually approach the target, their terminal LOS rate varies greatly and tends to disperse. Therefore, only Case 4 achieved a successful interception, whereas no collision courses have been achieved and the target escapes successfully in the other cases. This is due to the difficulty of the RCS and CBCG in effectively maintaining missiles' coverage situation when intercepting the highly maneuvering target. Therefore, the guidance law is vital for maintaining the credibility of the ETLs and the resulting intercept performance.

### 4.3. Robustness analysis

To further demonstrate the robustness and superiority of the proposed cooperative guidance strategy, the intercept effectiveness of multiple guidance strategies against a random step maneuver and random bang-bang maneuver target is analyzed in Case 7 and Case 8, respectively. The target random step maneuver and random bang-bang maneuver are expressed in Eqs. (39) and (40),

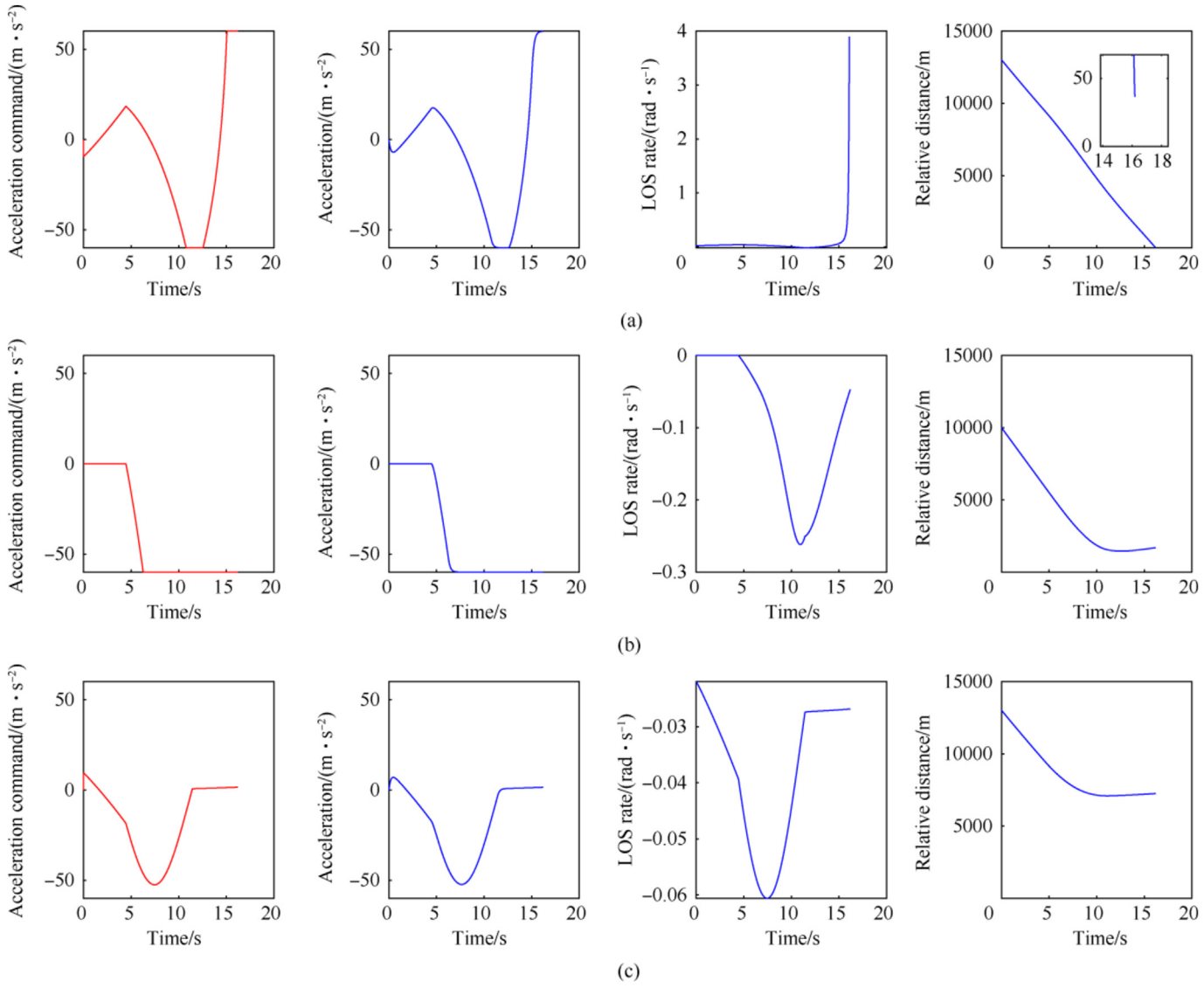


**Fig. 19.** Time history of commands, acceleration, LOS rate, and relative distance of the missile team in Case 5: (a) Missile $M_1$; (b) Missile $M_2$; (c) Missile $M_3$.

respectively, with a random amplitude $\mu$ and a random start time $\tau$.

$$a_T = \begin{cases} 0 & t-\tau < t_d \\ \mu a_{T,\max} & t-\tau \geq t_d \text{ and } \left|\theta_T - \theta_{T_0}\right| \leq \Delta\theta_{T,\max} \\ 0 & t-\tau \geq t_d \text{ and } \left|\theta_T - \theta_{T_0}\right| > \Delta\theta_{T,\max} \end{cases} \tag{39}$$

$$a_T = \begin{cases} 0 & t-\tau < t_d \\ \mu a_{T,\max} \cdot \operatorname{sign}\left(\sin\left(\frac{\pi}{2}t\right)\right) & t-\tau \geq t_d \text{ and } \left|\theta_T - \theta_{T_0}\right| \leq \Delta\theta_{T,\max} \\ 0 & t-\tau \geq t_d \text{ and } \left|\theta_T - \theta_{T_0}\right| > \Delta\theta_{T,\max} \end{cases} \tag{40}$$

where $t_d$ represents the time at which the target detects the missile, i.e. $r_i = r_d$. represents the maneuver magnitude, the sign of $\mu$ represents the maneuver direction, and $\tau \in [0, 8]$ determines the starting time of the maneuver.

For comparison, the initial conditions for the RCS, CBCG, and APN are set to be the same as those for the SMCS, satisfying the necessary conditions for interception. To explore the guidance performance under various target maneuver parameters, $\mu$ and $\tau$ are uniformly selected within their respective ranges, with corresponding step lengths of 0.05 and 0.2, respectively. Thus, 1600 simulations are conducted for each guidance method.

The resulting miss distances (MDs) for Case 7 are plotted in Fig. 21. The interception probabilities can be obtained by calculating the ratio of the number of successful interceptions to the total number of simulations, which are 96.92%, 73.34%, 81.19%, and 74.59% for the SMCS, RCS, CBCG, and APN, respectively. With the same initial formation based on Eqs. (33) and (34), the proposed SMCS significantly outperforms the other methods. This is due to the fact that the other three methods lack consideration of situation assessment and maintenance, whereas the SMCS emphasizes maintaining advantageous situations.

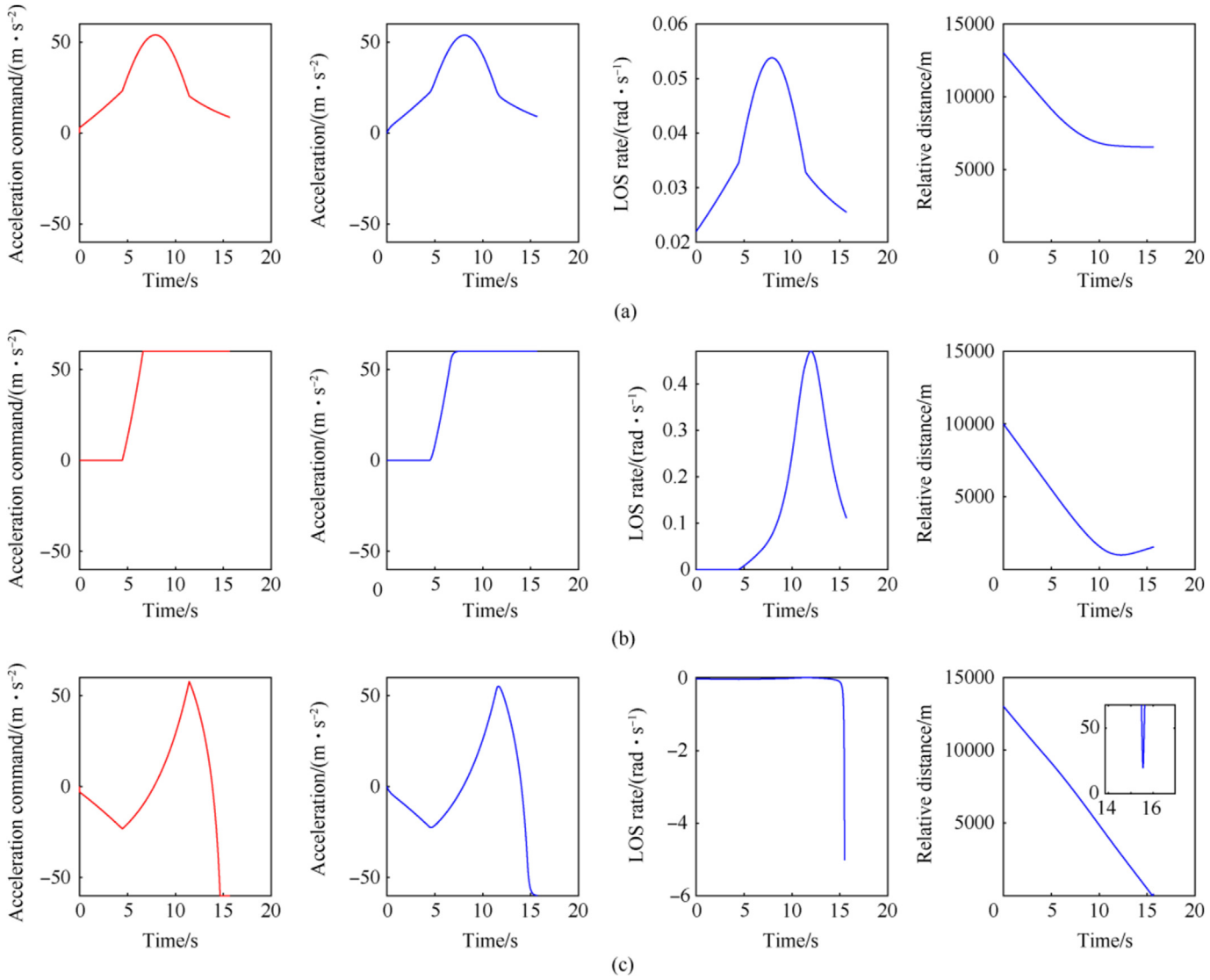


**Fig. 20.** Time history of commands, acceleration, LOS rate, and relative distance of the missile team in Case 6: (a) Missile $M_1$; (b) Missile $M_2$; (c) Missile $M_3$.

The MDs for Case 8 are shown in Fig. 22. The resulting interception probabilities are 83.95%, 68.77%, 73.63%, and 74.83% for SMCS, RSC, CBCG, and APN, respectively. The interception performance of all guidance strategies has decreased except for the APN. This is because the estimated target acceleration term adopted by the APN is assumed to be perfect, making it less sensitive to the acceleration variation of the bang-bang maneuver. Although the target acceleration term is also present in the first guidance stage of SMCS, it is intended to maintain an advantageous situation, whereas the APN directly uses the target acceleration term to eliminate miss distance. Due to different guidance strategies, the proposed SMCS performs the best against superior maneuvering targets.

### 4.4. Situation maintenance performance analysis

To verify the situation maintenance performance of the proposed strategy, the ETL introduced in subsection 2.3 is plotted for demonstration. Taking $\mu = 0.8$ and $\tau = 2.5$ s as an example in Case 7, the cooperative guidance trajectories for the RCS and SMCS are shown in Figs. 23 and 24, respectively.

Both strategies have the same ETLs at the initial moment (plotted in red solid line) and can cover the target's escape zone. However, as the situation changes during the interception process, the ETLs at $t_i = 10.43$ s (plotted in blue solid line) of missile $M_1$ and $M_3$ using the RCS are truncated at the turning circle and cannot cover the gap between missile $M_2$'s reachable set (plotted in blue dashed line) and the target's reachable set (plotted in black dashed line). Therefore, the coverage performance of the RCS degrades and the corresponding necessary conditions for interception are disrupted. In contrast, the ETLs at $t_i = 10.43$ s (plotted in blue solid line) of the SMCS still cover the target's escape zone, and successful interception is achieved near the new ETL by missile $M_1$. This is due to the fact that the SMCS maintains coverage by pursuing virtual targets with angle constraints in the first guidance stage.

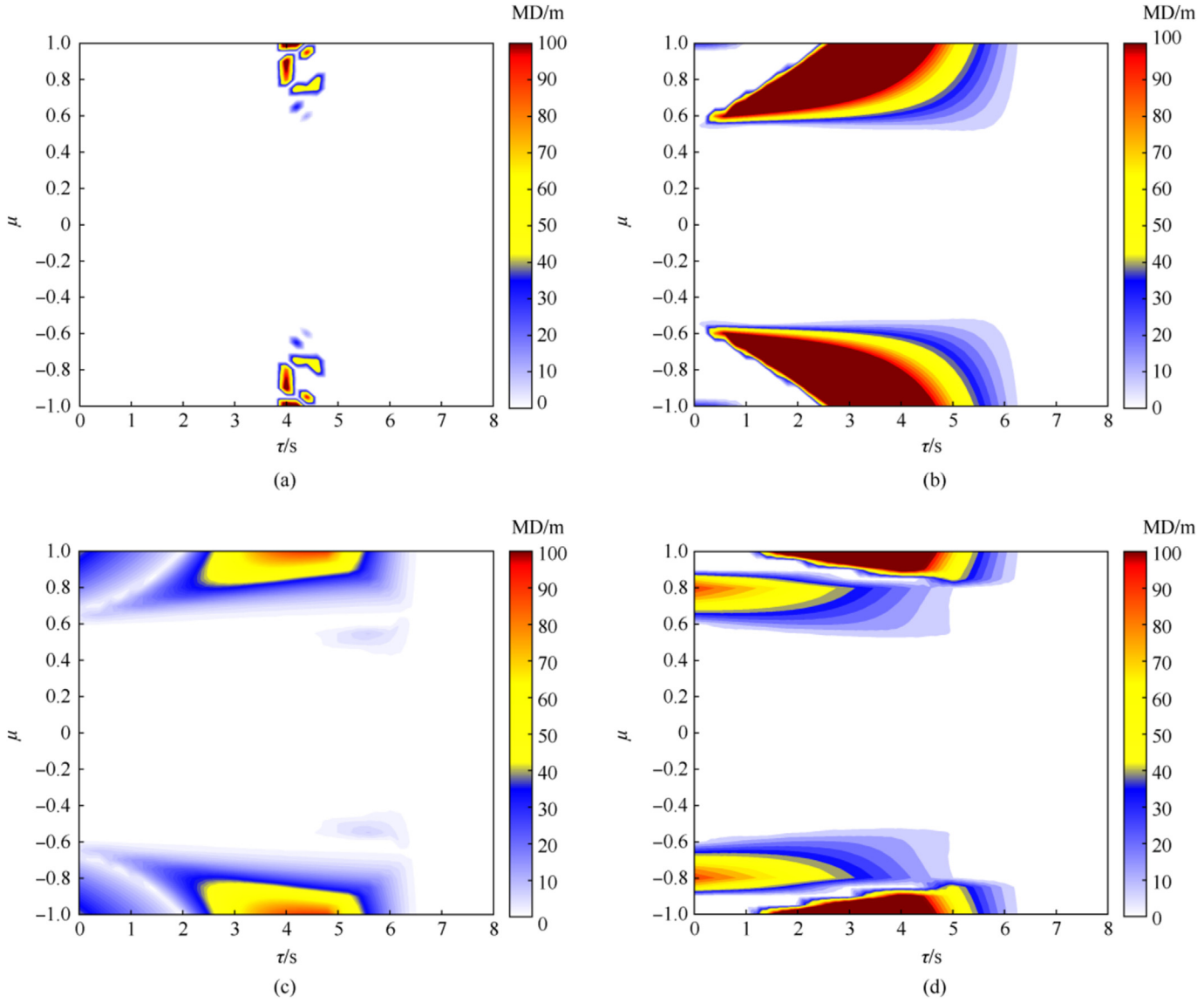


**Fig. 21.** Miss distance against random step maneuver (Case 7): (a) Miss distance of the SMCS; (b) Miss distance of the RCS; (c) Miss distance of the CBCG; (d) Miss distance of the APN.

## 5. Conclusions

This paper proposes a novel cooperative strategy for intercepting a highly maneuvering target via inferior missiles. The goal of the guidance strategy is to cooperatively cover the position that the target can reach with multiple missiles. Hence, engagement geometry analysis is performed based on the reachable set and reference frame. Then, an advantageous situation is derived and constructed by pursuing the virtual targets, while impact angle constraints are optimized to improve the maintenance of the collision triangle near impact. Numerical simulations demonstrate the high performance of the proposed strategy against targets executing constant, random step and bang-bang maneuvers. Future work can focus on a more complex engagement model involving three-dimensional kinematics and variable speeds of missiles and targets.

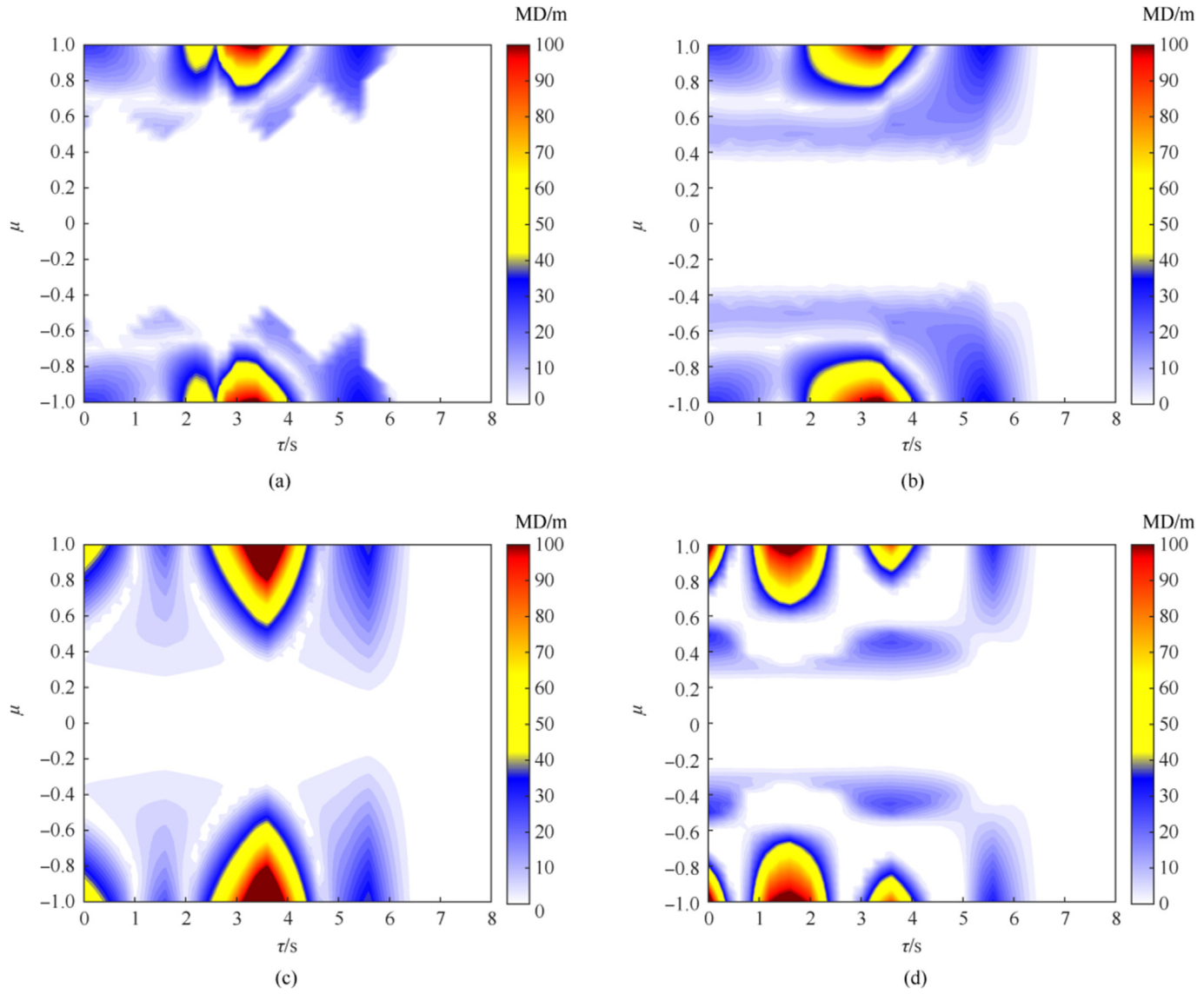


**Fig. 22.** Miss distance against bang-bang maneuver (Case 8): (a) Miss distance of SMCS; (b) Miss distance of RCS; (c) Miss distance of CBCG; (d) Miss distance of APN.

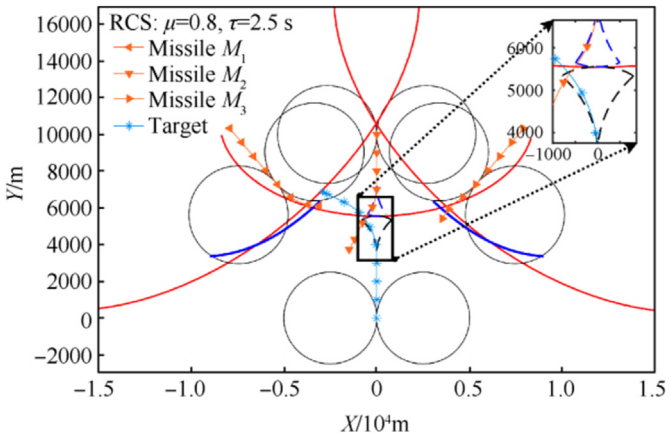


**Fig. 23.** Cooperative guidance trajectories via the RCS ($\mu = \mathbf{0.8}$ and $\tau = \mathbf{2.5\ s}$).

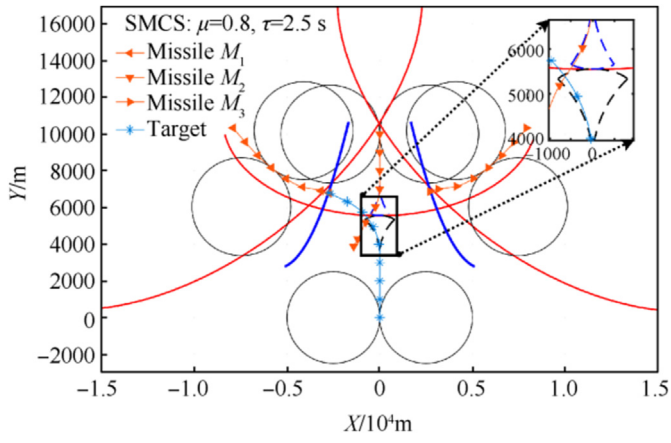


**Fig. 24.** Cooperative guidance trajectories via the SMCS ($\mu = \mathbf{0.8}$ and $\tau = \mathbf{2.5\ s}$).

## CRediT authorship contribution statement

**Xinghui Yan:** Supervision, Investigation, Formal analysis, Conceptualization. **Yuzhong Tang:** Writing – original draft, Methodology, Investigation, Formal analysis, Data curation. **Heng Shi:** Writing – review & editing, Supervision, Methodology, Investigation, Formal analysis, Conceptualization. **Yulei Xu:** Visualization, Validation, Software, Methodology. **Yiding Liu:** Validation, Investigation, Formal analysis.

## Declaration of competing interest

The authors declare that they have no known competing financial interests or personal relationships that could have appeared to influence the work reported in this paper.

## Acknowledgements

This work was supported by the National Natural Science Foundation of China (Grant No. 62203362) and the Natural Science Basic Research Program of Shaanxi (Grant No. 2023-JC-QN-0569).

## References

[1] Fan H, Yan J. Evolution and development trend of air combat system. Acta Aeronautica Astronautica Sinica 2022;43:269–305. https://doi.org/10.7527/S1000-6893.2022.27397.
[2] Zhu J, Kuang M, Zhou W, Shi H, Zhu J, Han X. Mastering air combat game with deep reinforcement learning. Defence Technology 2024;34:295–312. https://doi.org/10.1016/j.dt.2023.08.019.
[3] Cottrell RG. Optimal intercept guidance for short-range tactical missiles. AIAA J 1971;9:1414–5. https://doi.org/10.2514/3.6369.
[4] Weiss M, Shima T. Minimum effort pursuit/evasion guidance with specified miss distance. J Guid Control Dynam 2016;39:1069–79. https://doi.org/10.2514/1.G001623.
[5] Dun X, Li J, Cai J. Optimal guidance law for intercepting high-speed maneuvering targets. J Natl Univ Def Technol 2018;40:176–82. https://doi.org/10.11887/j.cn.201801027.
[6] Anderson GM. Comparison of optimal control and differential Game intercept missile guidance laws. J Guid Control 1981;4:109–15. https://doi.org/10.2514/3.56061.
[7] Zhang P, Fang Y, Zhang F, Xiao B, Hu S, Zong S. An adaptive weighted differential Game guidance law. Chin J Aeronaut 2012;25:739–46. https://doi.org/10.1016/S1000-9361(11)60440-8.
[8] Wang Y, Ning G, Wang X, Hao M, Wang J. Maneuver penetration strategy of near space vehicle based on differential game. Acta Aeronautica Astronautica Sinica 2020;41:69–78. https://doi.org/10.7527/S1000-6893.2020.24276.
[9] Liu F, Dong X, Li Q, Ren Z. Robust multi-agent differential games with application to cooperative guidance. Aero Sci Technol 2021;111:106568. https://doi.org/10.1016/j.ast.2021.106568.
[10] Liu F, Dong X, Li Q, Ren Z. Cooperative differential games guidance laws for multiple attackers against an active defense target. Chin J Aeronaut 2022;35:374–89. https://doi.org/10.1016/j.cja.2021.07.033.
[11] Chao T, Wang X, Wang S, Yang M. Linear-quadratic and norm-bounded differential game combined guidance strategy against active defense aircraft in three-player engagement. Chin J Aeronaut 2023;36:331–50. https://doi.org/10.1016/j.cja.2023.04.012.
[12] Wang X, Yang M, Wang S, Hou M, Chao T. Linear-quadratic and norm-bounded combined differential game guidance scheme with obstacle avoidance for attacking defended aircraft in three-player engagement. Defence Technology 2024. https://doi.org/10.1016/j.dt.2024.06.018.
[13] Gong X, Chen W, Lei W, Wang J, Chen Z, Li Y. Analytical game strategies for active UAV defense considering response delays. Defence Technology 2024. https://doi.org/10.1016/j.dt.2024.07.001.
[14] Hu Q, Han T, Xin M. Sliding-mode impact time guidance law design for various target motions. J Guid Control Dynam 2019;42:136–48. https://doi.org/10.2514/1.G003620.
[15] Ma P, Zhao Z, Chen S, Guo Y. Nonlinear active disturbance rejection guidance law for highly maneuvering targets. Control Theory and Technology 2023;40:942–8. https://doi.org/10.7641/CTA.2021.10239.
[16] Chen Y, Wu S, Wang X, Zhang D, Jia J, Li Q. Time and FOV constraint guidance applicable to maneuvering target via sliding mode control. Aero Sci Technol 2023;133:108104. https://doi.org/10.1016/j.ast.2023.108104.
[17] Wang C, Ding X, Wang J, Shan J. A robust three-dimensional cooperative guidance law against maneuvering target. J Franklin Inst 2020;357:5735–52. https://doi.org/10.1016/j.jfranklin.2020.03.007.
[18] Chung CF, Furukawa T. A reachability-based strategy for the time-optimal control of autonomous pursuers. Eng Optim 2008;40:67–93. https://doi.org/10.1080/03052150701593133.
[19] Su W, Li K, Chen L. Coverage-based cooperative guidance strategy against highly maneuvering target. Aero Sci Technol 2017;71:147–55. https://doi.org/10.1016/j.ast.2017.09.021.
[20] Su W, Shin H-S, Chen L, Tsourdos A. Cooperative interception strategy for multiple inferior missiles against one highly maneuvering target. Aero Sci Technol 2018;80:91–100. https://doi.org/10.1016/j.ast.2018.06.026.
[21] Yan X, Kuang M, Zhu J, Yuan X. Reachability-based cooperative strategy for intercepting a highly maneuvering target using inferior missiles. Aero Sci Technol 2020;106:106057. https://doi.org/10.1016/j.ast.2020.106057.
[22] Liu S, Yan B, Zhang T, Zhang X, Yan J. Coverage-based cooperative guidance law for intercepting hypersonic vehicles with overload constraint. Aero Sci Technol 2022;126:107651. https://doi.org/10.1016/j.ast.2022.107651.
[23] Hui Y, Nan Y, Chen S, Ding Q, Wu S. Dynamic attack zone of air-to-air missile after being launched in random wind field. Chin J Aeronaut 2015;28:1519–28. https://doi.org/10.1016/j.cja.2015.08.013.
[24] Sun Y, Wang X, Wang T, Gao P. Modeling of Air-to-air missile dynamic attack zone based on Bayesian Networks. Chinese Automation Congress (CAC); 2020. p. 5596–601. https://doi.org/10.1109/CAC51589.2020.9327613.
[25] Wang S, Guo Y, Wang S, Wang L, Tao Y, Peng Z. Capurability analysis for arbitrarily high-speed maneuvering targets. Chin J Aeronaut 2023;36:375–90. https://doi.org/10.1016/j.cja.2023.06.025.
[26] Li K, Bai Z, Shin H-S, Tsourdos A, Tahk M-J. Capturability of 3D RTPN guidance law against true-arbitrarily maneuvering target with maneuverability limitation. Chin J Aeronaut 2022;35:75–90. https://doi.org/10.1016/j.cja.2021.10.004.
[27] Su W, Li K, Chen L. Coverage-based three-dimensional cooperative guidance strategy against highly maneuvering target. Aero Sci Technol 2019;85:556–66. https://doi.org/10.1016/j.ast.2018.08.023.
[28] Zhang B, Zhou D, Li J, Yao Y. Coverage-based cooperative guidance strategy by controlling flight path angle. J Guid Control Dynam 2022;45:972–81. https://doi.org/10.2514/1.G006504.
[29] Guo Z, Xu T, Zhang Z, Duan Z. Cooperative covering guidance strategy design: a virtual targets approach. CCDC); 2021. p. 6987–92. https://doi.org/10.1109/CCDC52312.2021.9602267. 2021 33rd Chinese Control and Decision Conference.
[30] Guo Z, Xu T, Zhang Z, Duan Z. Designing cooperative covering strategy for intercepting a highly maneuvering target. IFAC-PapersOnLine 2022;55:149–53. https://doi.org/10.1016/j.ifacol.2022.05.026.
[31] Ramana MV, Kothari M. Pursuit strategy to capture high-speed evaders using multiple pursuers. J Guid Control Dynam 2017;40:139–49. https://doi.org/10.2514/1.G000584.
[32] Jeon I-S, Cho H, Lee J-I. Exact guidance Solution for maneuvering target on relative virtual frame Formulation. J Guid Control Dynam 2015;38:1330–40. https://doi.org/10.2514/1.G000932.
[33] Li H, Wang J, He S, Lee C-H. Nonlinear optimal impact-angle-constrained guidance with Large initial heading error. J Guid Control Dynam 2021;44:1663–76. https://doi.org/10.2514/1.G005868.
[34] Tang X, Yu J, Dong X, Ren Z. Integrated guidance and control with impact angle and general field-of-view constraints. Aero Sci Technol 2024;144:108809. https://doi.org/10.1016/j.ast.2023.108809.
[35] Robb M, White B, Tsourdos A. Earliest intercept line guidance: a novel concept for improving Mid-course guidance in area air defence. AIAA guidance, navigation, and control Conference and Exhibit, American Institute of Aeronautics and Astronautics; n.d. https://doi.org/10.2514/6.2005-5971.
[36] Shi H, Chen Z, Zhu J, Kuang M. Model predictive guidance for active aircraft protection from a homing missile. IET Control Theory & Appl 2022;16:208–18. https://doi.org/10.1049/cth2.12218.
[37] Hou L, Luo H, Shi H, Shin H-S, He S. An optimal geometrical guidance law for impact time and angle control. IEEE Trans Aero Electron Syst 2023;59:9821–30. https://doi.org/10.1109/TAES.2023.3305974.
[38] Zhao J, Zhou R. Unified approach to cooperative guidance laws against stationary and maneuvering targets. Nonlinear Dyn 2015;81:1635–47. https://doi.org/10.1007/s11071-015-2096-z.
[39] Chen Z, Wang K, Shi H. Elongation of curvature-bounded path. Automatica 2023;151:110936. https://doi.org/10.1016/j.automatica.2023.110936.
[40] Wu Z, He S, Wang Y, Li H. Nonlinear observability-enhancement optimal guidance law for moving targets. Acta Aeronautica Astronautica Sinica 2023;44:373–86. https://doi.org/10.7527/S1000-6893.2023.29750.